

1 Peer review status:

2

3 This is a non-peer-reviewed preprint submitted to EarthArXiv

4

5

6

7 **Characterization and Meteorological Drivers of Dust Events over California's Central**
8 **Valley**

9 **Precious Ebiendele¹ Adeyemi A. Adebisi¹, John T. Abatzoglou¹, Karin Ardon-Dryer²,**
10 **Md. Minhazul Kibria¹ and Cade Hogle²**

11 ¹School of Engineering, University of California, Merced, Merced, CA.

12 ²Department of Geosciences, Atmospheric Science Group, Texas Tech

13

14

15

16

17

18

19

20

21

22

23

24

25

26

27

28

29

30

31

32

33

34

35

36

37

38

39 **Abstract**

40 Dust events in California’s Central Valley pose severe risks to public health, regional air quality,
41 and transportation. Yet, the climatology and meteorological drivers of dust events in the region are
42 poorly characterized due to sparse monitoring and limitations of satellite observations. Using
43 meteorological observations from 15 Automated Surface Observation System stations, we
44 systematically catalog and analyze dust events across the Central Valley during 2005-2024,
45 leveraging a hybrid approach that combines observer-reported dust codes with meteorological
46 criteria that capture events missed by manual reporting, including those under cloudy and
47 nighttime conditions. We identified 707 dust events, averaging ~35 dust events per year and
48 increasing by $4.4 \pm 1.5\%$ per year since 2005. These dust events are generally short-lived (≤ 1 h in
49 ~78% of cases), occur mainly in the afternoon hours (14:00-18:00 local time), and are most
50 frequent in the southern San Joaquin Valley between September and November. Self-organizing
51 map analysis during the September-November peak dust season reveals four dominant synoptic-
52 scale configurations driving dust events, characterized by anomalously strong surface winds, low
53 relative humidity, and amplified mid-tropospheric troughs. Specifically, positively tilted troughs
54 with northwesterly surface winds produced widespread dust events during abnormally dry to
55 drought conditions, while negatively tilted troughs are associated with convective-driven fronts.
56 Our results provide a robust foundation for improving dust forecasting and public health
57 interventions in the agriculturally intensive Central Valley, experiencing intensifying drought and
58 land-use pressures.

59
60
61
62
63
64
65
66
67
68
69
70
71
72
73
74
75
76
77
78

79 **1. Introduction**

80 Air pollution is a significant challenge in many parts of California, particularly within the Central
81 Valley, which consistently ranks among the regions with the worst air quality in the United States
82 (American Lung Association, 2025). This region frequently violates California and National
83 Ambient Air Quality Standards for both fine particulate matter (PM_{2.5}) and ozone (e.g., EPA,
84 2018; SJVAPCD, 2025), resulting in severe public health impacts (e.g., Ha et al., 2024; Khanum
85 et al., 2021; Wang et al., 2019; Zarate-Gonzalez et al., 2024) and impacts on agriculture (Zeeshan
86 et al., 2024). Previous studies have shown that the Central Valley's severe air pollution results from
87 the synergistic interactions of unfavorable topography, meteorology, and anthropogenic emissions
88 (Chow et al., 2006; Zhao et al., 2011). Specifically, an enclosed basin bounded by the Sierra
89 Nevada and Coast Ranges restricts horizontal air movement (e.g., Leighton, 1966; Young et al.,
90 2016). This configuration leads to poor meteorological dispersion, particularly during stagnant
91 high-pressure systems that promote inversions and trap pollutants near the surface (e.g., Beaver &
92 Palazoglu, 2009; LaDochy & Witiw, 2023). Furthermore, these factors are exacerbated by
93 anthropogenic emissions from agricultural activities, emissions from both local and upwind
94 transportation and oil and gas extraction, and urban centers (Almaraz et al., 2018; Angevine et al.,
95 2013).

96 Unlike the conditions associated with chronic air quality issues in the Central Valley, characterized
97 by stagnant air masses, dust storms have occasionally impacted the region coincident with strong
98 winds, causing significant transportation hazards (Pauley et al., 1996) and air quality concerns.
99 Recent dust events in the region have taken on varying forms, from the widespread dust storm on
100 October 11, 2021, to a haboob-like event on November 11, 2024 (Fig. 1; NWS Hanford, 2024;
101 Edwards, 2024). Dust events in the Central Valley, a semi-arid to Mediterranean climate region,
102 are primarily driven by wind erosion, where strong winds entrain and transport soil particles in the
103 atmosphere (Zuo et al., 2024), drastically reducing visibility (Bhattachan et al., 2019). Specifically,
104 the primary dust emission mechanism is saltation bombardment (Kok et al., 2012), where saltating
105 sand grains over a surface bombard loose particles, breaking soil aggregates into smaller dust
106 particles that are eventually ejected into the atmosphere (Gillette et al., 1979; Shao, 2008). In
107 addition to the prevailing winds, dust emission also depends on environmental factors, including
108 soil moisture, surface roughness, vegetation cover, and atmospheric stability (Hennen et al., 2023;
109 Klose et al., 2014; Pu & Ginoux, 2017). These factors influence dust events in California's Central
110 Valley, where unvegetated and agricultural lands are susceptible to wind erosion (e.g., Kolesar et
111 al., 2022). Dust events have increased in the Central Valley in recent decades (Adebiyi et al., 2025;
112 Evan et al., 2025; Tong et al, 2017), potentially by underlying changes in these environmental
113 factors as well as changes in synoptic circulation patterns that frequently enhance surface winds
114 and boundary-layer mixing.

115 The contributions of wind-blown dust and dust storms to the Central Valley's air pollution have
116 often been underestimated (e.g., Cisneros et al., 2017; David et al., 2021). In addition, dust events
117 in the Central Valley have been associated with Valley Fever (coccidioidomycosis) – a fungal lung
118 infection caused by inhaling spores of the *Coccidioides* fungus, which primarily resides in

119 agricultural soil (Tong et al., 2023). California has recently seen a significant increase in Valley
120 fever cases, with reports rising from fewer than 1,000 in 2000 to a record high of 12,500 in 2024
121 (CDPH, 2025). Among these cases, the counties in the San Joaquin Valley (southern part of the
122 broader Central Valley) consistently report the highest counts of valley fever cases in the state.

123 Despite the critical consequences of dust events on public health, there is limited information in
124 the literature about dust events in the Central Valley. These include the characterization of dust
125 events and their synoptic drivers. In addition, there is a scarcity of monitoring stations capable of
126 characterizing these dust events. Of the 20 active California Interagency Monitoring of Protected
127 Visual Environments (IMPROVE) air quality monitoring stations used to measure fine dust
128 concentrations (e.g., Hand et al., 2017), only one is in the middle of the Central Valley, where the
129 majority of dust events occur (Ballard et al., 2008). While there are several Environmental
130 Protection Agency (EPA), the California Air Resources Board (CARB), and local air districts
131 monitoring stations that measure PM_{2.5}, very few measure PM₁₀, and these few stations cannot
132 discriminate between dust and other coarse-mode pollutants that constitute PM₁₀ (e.g., Chow et
133 al., 1993). Even when available, these stations are far apart and often located near major cities,
134 making it challenging to observe numerous small-scale dust events that are common in the rural
135 agricultural areas of the Central Valley (Young et al., 2025). While remote-sensing observations,
136 such as from satellites, have been used to capture these dust events (Adebiyi et al., 2025; Ginoux
137 et al., 2012), they are associated with very coarse resolution (typically greater than 10 km) and
138 other retrieval uncertainties, since these satellite sensors cannot directly observe dust (Castellanos
139 et al., 2024).

140 To address this gap, we systematically catalog and characterize dust events in the California
141 Central Valley using surface observations from Automated Surface Observation Systems (ASOS)
142 from 2005 to 2024. Unlike satellites or sparse IMPROVE networks, ASOS reports high-temporal-
143 resolution present-weather codes alongside meteorological measurements such as visibility, wind
144 speed and gust, relative humidity, and event-triggered sub-hourly (SPECI) special reports,
145 allowing precise timing of dust event duration even at night and under cloud cover. This automated
146 station-based design also offers significant added value over historical dust storm catalogs,
147 particularly the NOAA Storm Event Database (SED), due to reporting inconsistencies (Ardon-
148 Dryer et al., 2023). Because SED dust reports rely on non-meteorological human observers and
149 disparate sources, they often misclassify dust events and leave significant spatial and temporal
150 gaps.

151 Here, we quantify the climatology of dust events in the Central Valley, including their spatial and
152 seasonal patterns. We also explore recent trends in dust events during 2005-2024 and their
153 interannual relationships with drought conditions. Finally, we examine the meteorological patterns
154 associated with dust events in the Central Valley. Efforts to identify large-scale meteorological
155 patterns associated with dust events can help refine local forecasts and early warning systems to
156 mitigate dust-related hazards. By systematically characterizing when, where, and how dust events
157 develop in this region, this study aims to fill a current research gap and provide a foundation for

158 improved dust event prediction, support targeted public health interventions, transportation safety
159 policies, and control mitigation strategies as climate change and land-use pressures heighten
160 regional dust activity.

161

162 **2 Methods and Materials**

163 **2.1 Meteorological Observation Stations**

164 Our study used station-based meteorological observations from the Automated Surface
165 Observation System (ASOS) and Automated Weather Observing System (AWOS) networks
166 operated by the U.S. National Weather Service and Federal Aviation Administration (Landolt et
167 al., 2019). As a result, these observing stations are often located at the airport and adhere to World
168 Meteorological Organization (WMO) standards. These datasets comprise continuous quality-
169 controlled surface weather observation stations across the US, and an array of sensors (see NOAA,
170 1998) produce these data, and the resulting sensor signals are processed using several automated
171 algorithms (e.g., visibility algorithm, obscuration algorithm, single-site lightning sensor algorithm,
172 and precipitation identification algorithm) that automatically report core Meteorological
173 Aerodrome Report (METAR) elements (Cook et al., 2023; Landolt et al., 2019).

174 We used 15 meteorological stations (Table S1) spanning the Central Valley and covering 20 years
175 from January 1st, 2005, to December 31st, 2024 (Fig. 2a). We obtained these datasets through a
176 Python API from the Iowa Environmental Mesonet archive (<https://mesonet.agron.iastate.edu>) and
177 converted them to local time. Each station reports visibility, wind speed and direction (including
178 gusts), temperature, dew point, precipitation, sea-level pressure, and present weather codes (e.g.,
179 thunderstorms, rain, haze, and dust) at a time resolution of 5-minute intervals through METAR
180 messages (Horel et al, 2002). We note that these stations report relative humidity (RH) at hourly
181 intervals. To obtain sub-hourly RH consistent with our 5-minute analysis, we computed RH at
182 each METAR issuance time using the air temperature (T) and dew-point temperature (Td) encoded
183 in the METAR text.

184

185 **2.2 Identification of dust event**

186 Although the ASOS/AWOS systems can automatically identify precipitation types and some
187 obscurations, such as fog, they lack sensors to distinguish airborne dust from other particulate
188 matter (NOAA, 1998). Instead, atmospheric dust particles affect these meteorological stations'
189 measurements indirectly by reducing visibility, which the station may report as haze (HZ), unless
190 an observer overrides it with a specific dust code (NOAA, 1998; Xi, 2020). These specific dust
191 codes include "DU", which is widespread dust in the air; "BLDU", which is blowing dust at the
192 station, resulting in an intermediate visibility drop of a few kilometers, DS, which are dust storms
193 that typically reduce visibility to below about 1 km (WMO, 2019), and "SS", which are sandstorm.
194 These dust codes are not automatically encoded in the record and require trained weather observers
195 to enter each code manually. In practice, many of these stations operate in fully automated mode

196 most of the time, using optical sensors that cannot distinguish dust from fog or haze, so dust events
197 often go into the record without an explicit “dust” label, appearing only as lowered visibility with
198 an HZ label.

199 Therefore, to adequately characterize all dust events at the stations, we selected 5-minute dust
200 cases using the following procedures (Figure S1): First, we selected all dust cases that were
201 manually recorded with single weather codes, DU, BLDU, DS, and SS, as well as cases with other
202 weather codes, but included these dust codes. Second, because not all dust events have recorded
203 dust codes (e.g., the case study on November 11, 2024, which is recorded with an HZ label despite
204 a visible dust event; see Fig. 1b-e), we also identified dust cases using observed meteorological
205 parameters (Robinson & Ardon-Dryer, 2024). ASOS/AWOS automatically reports HZ as an
206 obscuration during low visibility (<10km) and dry conditions (dew point depression > ~4° F)
207 without precipitation, which is frequently observed in the Central Valley. Because HZ is not
208 uniquely attributable to dust, using HZ alone may bias observer-coded dust frequency estimates.
209 Therefore, we apply additional stringent criteria to treat HZ as dust (dusty-HZ) when it meets the
210 meteorological conditions below: (a) Wind speed > 6 m/s; (b) Visibility drops < 10 km; and (c)
211 RH < 70%. For these cases, we use a wind speed greater than 6 m/s because previous studies have
212 suggested that this value is a realistic lower threshold for saltation and, by extension, dust uplift
213 (Bagnold, 1941). In addition, we used a visibility threshold of less than 10 km, as defined by the
214 WMO (WMO, 2019), for blowing dust and dust storms. Further, we used RH less than 70% to
215 remove cases that are associated with fog or widespread precipitation. In addition to the
216 meteorological criteria, we further added an extra layer of screening for both (a) dusty-HZ cases
217 that meet the meteorological conditions and (b) cases with manual dust codes (DU, DS, BLDU,
218 SS). Specifically, we removed cases with any occurrence of wildfire smoke (FU) or mist (BR)
219 conditions within a ± 2 hours window before and after the recorded drop in visibility to ensure
220 that any reduction in visibility is most likely due to dust events (Suarez-Molina et al., 2024).

221 In addition, we confirmed suspected dusty-HZ cases by leveraging the Geostationary Operational
222 Environmental Satellite (GOES) and National Weather Service (NWS) reports, as well as PM10
223 concentration measurements and smoke or wildfire-reported cases. For each HZ observation that
224 meets our screening criteria above for dust, we first examined the corresponding satellite visible
225 imagery within 1 hour of the report to visually assess whether dust was present. Second, we
226 reviewed NWS products, including Area Forecast Discussions and special weather statements.
227 Any explicit mention of blowing dust, reduced visibility due to dust, or a blowing dust advisory in
228 the station county or along adjacent transport corridors served as additional confirmation. Finally,
229 we examined PM10 concentration at air quality stations closest to the ASOS/AWOS stations
230 (Table S2) to assess if there was an increase during an identified dust episode (i.e., from the first
231 identified dust-coded ASOS/AWOS report to the last dust-coded report, with an added ± 2 -hour
232 buffer to capture onset and end). However, when wildfire smoke is reported during the same
233 period, we do not use the PM10 increase as supporting evidence for dust and often discard such
234 dusty-HZ cases. With the above procedure, we identified 5,251 station-level dust observations,
235 defined here as individual ASOS/AWOS reports (recorded at the station’s native cadence) that

236 were classified as dust based on the present weather codes (PWC) and /or our dusty-HZ screening
237 criteria. Among these cases, 11.9% have at least one recorded dust code (i.e., DU, BLDU, DS, or
238 SS), and the remaining 88.2% are dusty-HZ (Fig. 2).

239 We grouped dust observations into station-level dust events. A *dust event* at a station is defined as
240 either (a) a single dust observation (visibility ≤ 10 km), or (b) a sequence of consecutive dust
241 observations at a station, evaluated at the station's native reporting cadence (e.g., 5-min or hourly),
242 with no intervening non-dust observations. Observations included in an event must have visibility
243 below 16km (including at least one observation with visibility ≤ 10 km) and indicate dust either
244 through dust codes (DU/BLDU/DS/SS) or dusty-HZ conditions. Thus, if a station records a single
245 dust observation (visibility ≤ 10 km), we retain it as a dust event of one reporting interval. This
246 avoids discarding short-lived events that may only be captured once in hourly reports. To avoid
247 overcounting, we treat dust events that begin near midnight local time and persist into the following
248 day as a single continuous event rather than two separate events. We also count as separate events
249 if they occur at different times of the day and are separated by at least 2 hours (e.g., an event that
250 occurs in the morning and another that occurs in the evening are counted as two separate events).
251 Multiple dust events on the same calendar day at a given station were uncommon (e.g., only 6.4%
252 of days in which a station recorded at least one dust event contained more than one event).
253 Characterization of identified dust is summarized at three levels: (a) dust observations: individual
254 ASOS/AWOS reports meeting our dust criteria, (b) station-level dust events, and (c) dusty days:
255 calendar days on which at least one station in the Central Valley reports a dust event. To derive
256 regional statistics, the total number of identified dust events in the Central Valley is computed as
257 the sum of station-level dust events across all stations over the study period (2005-2024), while
258 the total number of dusty days is computed as the count of calendar days during 2005 to 2024 on
259 which at least one Central Valley station reports a dust event.

260 Trends in annual dust events were estimated using ordinary least squares regression applied to the
261 regional annual time series (i.e., the number of dust events summed across all stations each year).
262 Uncertainty is reported as ± 1 the standard error of the fitted slope. In addition, to check for
263 consistency between our identified station base dust event and satellite regional-scale measure of
264 atmospheric dust loading, we estimated column-integrated dust burden following Adebisi et al.,
265 (2025) using MODIS-derived dust optical depth.

266

267 **2.3 Upper-Level Meteorological Information from Reanalysis Dataset**

268 We used two complementary datasets to gain a deeper understanding of the synoptic patterns and
269 drivers of dust events in California's Central Valley: the European Centre for Medium-Range
270 Weather Forecasts' ERA5 reanalysis (Hersbach et al., 2020) and the North American Rapid
271 Refresh version 3 (RAPv3; Benjamin et al., 2016). First, we use ERA5 to construct dusty-day
272 composites of surface wind, relative humidity, 500-hPa geopotential height (z500), volumetric soil
273 water in the surface layer (0-7cm), and total cloud cover at hourly resolution (2005 to 2024). For
274 the composite analysis, we restrict the sample to *widespread dusty days*, defined as any day (UTC)

275 when dust events were seen over at least 20% of stations in the Central Valley. We use this
276 definition to reduce the influence of highly localized events that are unlikely to reflect a coherent
277 synoptic-scale circulation.

278 Second, we further consider two diagnostic case studies (see Fig. 1; 11 October 2021 and 11
279 November 2024) using RAPv3 because it provides higher spatial resolution (13 km horizontal
280 grid) and better resolves mesoscale gradients and near-surface wind maxima relevant for dust
281 emission than the ERA5 reanalysis. RAPv3 uses the WRF-ARW model with a hybrid ensemble
282 variational data assimilation scheme, ingesting frequent observations (e.g., radar reflectivity,
283 cloud, and surface data). The benefits of high-resolution RAPv3 are that it can capture the
284 evolution and spatial details of mesoscale dynamics in a rapidly changing atmosphere, such as
285 small-scale frontal boundaries, sharp moisture–dryline interfaces, lee-side surface cyclogenesis,
286 convective cold-pool surges, and jet streaks that entrain and transport dust. In contrast, ERA5's
287 coarse resolution often smoothed out these features. We used only the initialization hours of
288 RAPv3, and no forecast hours were used in this study. We obtained hourly geopotential height at
289 500 hPa (z500), relative humidity (RH500), 10m wind components (u10m, v10m), surface relative
290 humidity, near-surface temperature, wind speed, and surface pressure. Although RAPv3 has a
291 higher resolution than ERA5, we use ERA5 for our synoptic composite analysis because it
292 provides a temporally consistent match with our selected meteorological stations over the period
293 of interest (2005 to 2024), whereas RAPv3 only has records since 2012.

294 **2.4 Synoptic Pattern Classification: Self-Organizing Mapping (SOM)**

295 We applied a self-organizing map (SOM) clustering algorithm, a machine-learning approach, to
296 classify synoptic meteorological patterns associated with dust events in the Central Valley. We are
297 motivated to use SOM because dust events in the Central Valley result from different combinations
298 of large-scale synoptic patterns rather than a singular pattern. SOM maps high-dimensional input
299 data onto a predefined number of cluster centers through an iterative training process (Kohonen,
300 2002). Several previous studies (Li et al., 2023; Sweeney et al., 2017; Uotila et al., 2017) have
301 widely used this approach, including for capturing extreme events in data-limited contexts
302 (Cassano et al., 2015). Unlike traditional clustering methods, its ability to preserve the topological
303 relationships of the input data enables robust identification of recurring synoptic patterns (Sheridan
304 & Lee, 2011).

305 Here, we used SOM to cluster z500 from ERA5 over the broader Northeast Pacific and western
306 North America (30–50° N, 130–105° W) using the SOMoclu Python library (Wittek et al., 2017).
307 We composited only widespread events (as defined in Section 2.3). For each day, we identified
308 dust duration windows and computed the average daily dust window duration, which summarizes
309 event persistence across the SOM nodes. We trained each SOM with an epoch size of 1000 and
310 utilized a fixed random seed for reproducibility. After training, we identified the SOM's best-
311 matching unit and assigned it to a single node label. We tested several SOM grid sizes (e.g., 4, 6,
312 8 clusters) and found that 4 clusters (Type 1–4) yielded distinctly interpretable patterns, whereas
313 larger cluster sizes yielded redundant or transitional types. Of the identified widespread events, we

314 then quantified the frequency of each synoptic pattern and computed composite geopotential fields
315 by averaging all daily maps assigned to each type. In addition, spatial differences between types
316 were evaluated using grid-point Welch's t-tests on the composite fields, with significance assessed
317 at $p < 0.05$.

318

319 **2.5 Drought conditions**

320 To examine how drought conditions modulate dust events under an identified synoptic scale
321 pattern, we classify monthly dust events as a function of drought severity using the 1-month
322 Standardized Precipitation-Evapotranspiration Index (SPEI-1) from the National Oceanic and
323 Atmospheric Administration (NOAA) Climate Gridded Dataset (NClimGrid). Here, SPEI is based
324 on standardized anomalies in monthly climatic water balance (P-PET, where P is precipitation and
325 PET is potential evapotranspiration) using the Pearson Type III distribution. We spatially average
326 SPEI-1 over the Central Valley to obtain a regional drought indicator. In addition, we classified
327 months into drought categories using SPEI-1 thresholds (e.g., drought: $SPEI < -0.8$; abnormally
328 dry: $-0.79 < SPEI < -0.50$; normal dry: $-0.49 < SPEI < 0$, and no drought when $SPEI > 0$). To
329 estimate the sensitivity of dust events to drought conditions, we defined annual dry-month
330 frequency as the number of months per year with $SPEI-1 < 0$ and computed the Pearson correlation
331 between annual dust event totals and annual dry-month frequency across the study period.

332 To examine the timing of the first significant rainfall event in the Central Valley, we used daily
333 precipitation from the gridMET (Abatzoglou, 2013) gridded meteorological dataset ($1/24^\circ$; ~ 4 km
334 resolution). Because precipitation over the valley is spatially heterogeneous, we identify rainfall
335 onset using a spatial coverage metric. We first defined the onset of rainfall as the first Julian day
336 after September 1, when precipitation becomes spatially widespread across the Central Valley;
337 specifically, onset is the first day for which at least 50% of Central Valley grid cells receive
338 precipitation $\geq 1 \text{ mm day}^{-1}$ on at least 2 of 3 consecutive days (Taylor et al., 2025). To avoid
339 false onsets due to isolated early storms, we additionally required that at least one further
340 widespread wet day (again, $\geq 50\%$ of grid cells receiving $\geq 1 \text{ mm day}^{-1}$) occur within the
341 subsequent 14 days following the initial 3-day onset window. In addition, onset timing was
342 expressed as days since 1 September and categorized into early and late onset using a median onset
343 timing (i.e., 50th percentile of onset across the 2005-2024 period). Onsets occurring on or before
344 the median were classified as early onset, and seasons with onsets occurring after the median were
345 classified as late onset.

346 Furthermore, we quantified how dust is distributed across onset timing (early or late phase) and
347 drought categories (e.g., no drought, normal dry, abnormally dry, and drought) by computing the
348 fraction of dust events occurring in each onset-drought state. This describes how dust events are
349 distributed across the timing phases of rainfall conditional on dust occurrence.

350 Second, we assess whether drought conditions are associated with synoptic-scale patterns that
351 drive dust in the Central Valley. Specifically, we asked whether the relative occurrence of the four

352 SOM circulation types (Types 1-4) changes across dry conditions. To do this, we grouped dust
353 events by SPEI drought categories and SOM type and quantified how the seasonal mix of SOM
354 types (Types 1-4) varies.

355

356 **3.0 Results**

357 **3.1 Verification of Dust Criteria using Recent Case Studies**

358 To verify that our definition accurately captures the observed dust event, we show in Fig. 3 the
359 evolution of wind speed, visibility, relative humidity, and PM10 for the two case studies identified
360 in Fig. 1. As indicated in the section 2.2 above, we defined a dust event as a period when dust code
361 is identified or when the wind speed is more than 6 m/s, visibility is less than 10 km, and relative
362 humidity is less than 70 %, if no specific dust code identified. Although not all are defined by dust
363 codes, the above criteria identify a window of dust events that propagates southward in both cases.
364 For the October 11, 2021 case, the northern station at Stockton (SCK) shows the dust event starts
365 around 08:50 local time (LT), while the dust event starts about three hours later further south at
366 Porterville (PTV; Fig. 3a). Satellite observations confirm that this dust event occurs between 08:00
367 and 19:00 LT, as it traverses north to south across the entire Central Valley (Fig. S2), as do station-
368 based PM10 measurements. Unlike the October 11, 2021 case, the November 11, 2024 case was
369 not visible from the remote-sensing platforms due to cloud cover associated with a propagating
370 convective system (Fig. S3), but the dust storm preceding this system – a “haboob” – was captured
371 by the ground-based cameras (see Fig. 1b). Specifically, for the November 11, 2024 case, the
372 northern station at Merced (MCE) that captures the events starts around 12:25 LT, propagating
373 southward through the Porterville (PTV) at 15:45LT (Fig. 3b). In the absence of satellite
374 observation, we confirm this event by the ground-based EPA stations that shows sudden increases
375 in PM10 measurements as the convective system and the haboob dust event travel southward (see
376 purple lines in Fig. 3b). Overall, these results highlight the range of differences in dust events and
377 the advantage of ground-based identification, especially when cloud cover prevents remote
378 sensing.

379

380 **3.2 Climatology of Dust Events in the Central Valley**

381 Dust events in the Central Valley exhibit distinct annual, seasonal, and diurnal variabilities (Fig.
382 4). Between 2005 and 2024, we identify a total of 707 dust events, corresponding to ~ 35 events
383 yr^{-1} , spanning across 660 dusty days ($\sim 33 \text{ days yr}^{-1}$) (Fig. 2c and Fig. 4a). Most of these dust events
384 occur in the southern San Joaquin Valley, with the highest numbers recorded at HJO (Hanford
385 Municipal Airport) in Kings County and BFL (Meadows Field Airport) in Kern County each
386 averaging about 8 and 6 dust events yr^{-1} , respectively (Fig. 2c). In addition, relative to the average
387 during the period of record, annual dust events frequency in the Central Valley has increased by
388 $4.4 \pm 1.5\% \text{ yr}^{-1}$ during 2005-2024 (Fig. 4a). In addition, we also find that the correlation between
389 annual dust events and annual frequency of drought conditions (SPEI values less than 0) is 0.56 (p
390 < 0.05). While lack of rainfall is generally prevalent in the Central Valley, this result suggests that
391 drought conditions play a role in the interannual variability of dust events in the Central Valley

392 (see section 3.5 below). Consequently, the annual variability of station-based dust-event counts is
393 consistent with satellite-based estimates of column-integrated dust burden, suggesting that our
394 station-based assessment of dust events is representative of the entire Central Valley (see blue line
395 in Fig. S4).

396
397 Second, we also find that the seasonal cycle shows a peak in the number of dust events in October
398 (Fig. 4b). In addition, there is a secondary peak in dust events, with lower dust counts, in April-
399 June. In addition, this seasonal cycle of our identified dust events is consistent with the PM10
400 measurements recorded at locations near the identified ASOS/AWOS stations (Fig. S5). Similar
401 to the stations' dust counts, the PM10 measurements show a peak concentration in October,
402 approximately $91.3 \mu\text{gm}^{-3}$ during the dust events identified in Fig. 4, compared to the climatology
403 of $53.6 \mu\text{gm}^{-3}$ in the same month. For this seasonal cycle of dust events crossing the Central Valley,
404 wind speed is an important predictor, with its influence modulated by other parameters (see next
405 section and Fig. 5). For example, stronger winds during the core rainy season are likely to produce
406 fewer dust events because precipitation and higher soil moisture increase surface cohesion and
407 suppress dust emission. In contrast, the fall peak can be associated with the transition from
408 quiescent to more dynamic synoptic circulation patterns (see section 3.4 below) with seasonally
409 dry soils prior to the onset of winter precipitation (Lukovic et al., 2021) and potentially
410 compounded by seasonal farming activities (e.g., harvest, post-harvest).

411
412 Third, we also find that most of the dust events in the Central Valley occur during the daytime,
413 with the peak between 14:00 and 18:00 LT (Fig. 4c). This peak period also corresponds to the peak
414 daily temperature and resultant convective boundary layer turbulence, resulting in stronger surface
415 winds that are conducive to dust mobilization (Gunn et al., 2021). Regardless of the time of day
416 of the dust event, we find that about 78% of all identified dust events in the Central Valley occur
417 for one hour or less (Fig. 4d). Dust events exceeding five hours constituted only 1.4% of total
418 occurrences, with exceptionally long events (>10 hours) exceeding rare (1.7%). This
419 characterization of dust-event durations is largely consistent across all stations, with short-duration
420 dust events (≤ 1 hr) ranging from $\sim 50\%$ to 89% of all occurrences, and high-duration dust events
421 (> 1 hr) ranging from 11% to 50% of all occurrences (Fig. S6). In addition, higher numbers of
422 long-duration dust events occur more in the southern stations, where there are more overall dust
423 occurrences (see Fig. 2). For example, 30.4% and 23.9% of dust events in BFL and HJO,
424 respectively, are long-duration events (Fig. S5). Overall, the dominance of short-duration events
425 across stations is consistent with other reported studies in different dust-prone regions, such as the
426 southwestern United States (Robinson & Ardon-Dryer, 2024) and Phoenix, Arizona (Sandhu et
427 al., 2024).

428 **3.3 Local Meteorological Characteristics of Dust Events**

429 In addition to the distinct annual, seasonal, and diurnal variability, dust events also exhibit unique
430 local meteorological characteristics that differ from the baseline climatology during the same
431 period across stations in the Central Valley. Specifically, dust events tend to have stronger wind

432 speeds, lower visibility, and humidity when compared to the baseline climatology (Fig. 5). Our
433 result confirms that dust events occur during higher wind speeds, even when typical conditions are
434 calmer (Fig. 5a & d). On average, the wind speed during dust events is 5.6 m s^{-1} , higher than
435 climatology (8.2 m s^{-1} for dust and 2.6 m s^{-1} for climatology; Fig. 5a).

436 In addition to the wind speed, our result also shows that visibility and RH are generally lower
437 during dust events than climatological conditions (Fig. 5). Specifically, we find that, on average,
438 the visibility is lower by 7.9 km (8.1km for dust event and 16 km for climatology) and the RH by
439 22.1 % (33.7 % for dust event and 54.8% for climatology) during dust events than the climatology
440 across the stations in the Central Valley. While most dust events occur during higher wind speeds,
441 lower visibility, and RH than climatology, a small fraction occur at wind speeds less than 6 m/s,
442 visibility higher than 12 km, and RH higher than 70%. Our analysis indicates that most of these
443 cases involve defined dust codes (such as BLDU, DU, DS, and SS), suggesting these codes are
444 reported independently of our screening thresholds (which are applied only when dust codes are
445 absent, see Fig. S1) and can occasionally occur without a strong signal in screening variables.

446 The spatial distribution of these meteorological characteristics during dust events shows
447 substantial station-to-station variability across the Central Valley (Fig. 5d-f). Several stations in
448 the southern part exhibit generally higher wind speeds and lower RH during dust events. While
449 the strongest wind speeds during dust events occur at the Redding (RDD) in the north, this location
450 is likely influenced by mesoscale factors as wind accelerates through mountain gaps into the
451 Valley (see Fig. 2a), rather than large-scale synoptic drivers (see section 3.4 below). In addition,
452 five of the eight stations in the southern part of the Central Valley have mean visibility less than 7
453 km during dust events compared to only two in the northern part of the Central Valley. Like wind
454 speed, there is less spatial variability in mean RH in the southern than in the northern parts of the
455 Central Valley.

456

457 **3.4 Synoptic-scale Assessment of Dust Events in the Central Valley**

458 Like the station-based meteorological characteristics above, we also examine the differences
459 between the composite-mean of dust events and baseline climatology using ERA5 reanalysis. We
460 find that the differences across the entire Central Valley are similar to those characterized by the
461 meteorological stations (Fig. 6). Specifically, dust events are typically associated with stronger
462 wind speeds and lower RH than the climatology (Fig. 6a & b). Both station-level and valley-wide
463 diagnostics indicate a similar fingerprint but different amplitude, with larger station-level
464 anomalies ($\Delta U = +5.6 \text{ m/s}$; $\Delta RH = -22.1\%$; Fig 5) compared to the valley basin mean
465 composite ($\Delta U = +1.67 \text{ m/s}$; $\Delta RH = -13.90\%$; Fig 6). These changes in wind speed and RH
466 are influenced by synoptic factors including an upper-level low-pressure system (trough) just north
467 of California. This system, therefore, results in lower 500-mb geopotential height during dust
468 events than the baseline climatology (Fig. 6c). During the fall months with the highest dust events

469 (September-November), this type of system often dominates the synoptic-scale pattern,
470 influencing the meteorological characteristics that are conducive to dust mobilization (Fig. S6).

471 **3.4.1 Synoptic Categorization of Dust Events in the Central Valley**

472

473 Our SOM analysis yielded four (4) dominant synoptic configurations (Types) that influence
474 widespread dusty days in the Central Valley (Fig. 7). The first configuration, representing 35.6%
475 of dust events (Type 1), shows a negatively tilted mid-tropospheric trough with the low-pressure
476 center over the northeastern Pacific Ocean, northwest of California. SOM mode 4 (Type 4;
477 accounting for 15.3% of dust events) also features a negatively tilted trough, but with the low-
478 pressure center over the Cascade Range. In contrast, Types 2 and 3 are both positively tilted mid-
479 tropospheric troughs, each accounting for 28.8% and 20.3% of dust events respectively. Although
480 both low-pressure centers are north-eastward of California, Type 2 has its low-pressure center
481 positioned further east, tilting it slightly more than Type 3. Unrelated to the tilt axis of the
482 geopotential fields, Type 1 and Type 3 are also associated with stronger pressure gradients at 500
483 mb than Type 4, with Type 2 showing similarly strong gradients. In addition, the synoptic
484 configurations patterns (Fig. 7a) are robustly distinct between Type 1 and Type 4, and between
485 Type 2 and Type 3, with statistically significant differences in z_{500} across much of the domain
486 ($p < 0.05$).

487

488 These differences in pressure gradient, tilt, and overall synoptic-scale configuration among the
489 configuration Types are linked to specific wind speed and direction at the surface, which influence
490 dust events (Fig. 7b-d and Fig. S8). Specifically, the average wind speeds for Type 2 and Type 3
491 are higher than those of Type 1 and Type 4. This is partly due to the orientation and direction of
492 surface winds, as well as the influence of the surrounding topography. For Type 1 and Type 4, the
493 winds are mainly westerly (with some southwesterlies in Type 1 and northwesterlies in Type 4),
494 but their speeds are usually damped by the Coastal Range. Conversely, the winds for Type 2 and
495 Type 3 tend to be more northwesterly to northerly, aligning more closely with the orientation of
496 the Central Valley, and the nearby topography offers less obstruction compared to Type 1 and
497 Type 4. Consequently, these winds are stronger, with a greater proportion exceeding 6 m/s (the
498 threshold for dust mobilization), than in the Type 1 and Type 4 synoptic configurations.
499 Additionally, stronger mid-tropospheric pressure gradients are associated with stronger surface
500 winds in the Central Valley, which are more evident in Type 2 and Type 3, than in Type 1.

501

502 In addition to the enhanced surface winds, these synoptic-scale configurations are also associated
503 with soil and atmospheric conditions that favor dust events. Specifically, we find that soil and
504 atmospheric conditions for Type 2 and Type 3 are drier than for Type 1 and Type 4 (Fig. 8 and
505 Fig. S8). While the Central Valley generally has drier soil than other parts of the state (Fig. S8b),
506 the anomalies for Type 1 and Type 4 show that soil water is higher than the September-November
507 climatology in northern California and some parts of the Central Valley. Unlike Type 4, which
508 shows positive soil water anomalies concentrated in northern California (including the northern

509 Central Valley), Type 1 shows positive anomalies mainly along far northern California, with much
510 of the Central Valley generally neutral or drier than climatology. In contrast, soil water in the San
511 Joaquin Valley and other southern parts of California is drier than the September-November
512 Climatology. This suggests that most of the dust events in Type 1 are more likely to occur in the
513 San Joaquin Valley than in the Sacramento Valley. Conversely, Type 2 and Type 3 have drier soil
514 water conditions throughout most of the Central Valley. Within the Central Valley, the driest soil
515 regions largely overlap with areas of predominantly strong wind speeds in the Sacramento Valley,
516 indicating that synoptic-scale configurations of Type 2 and Type 3 are most likely to facilitate dust
517 events in the Sacramento Valley.

518

519 Using RH and cloud cover as proxies, our results further show a consistent pattern of atmospheric
520 moisture across the Central Valley and the state, similar to soil water distribution. The RH for
521 Type 2 and Type 3 is generally lower than for Type 1 and Type 4. Additionally, Type 1 and Type
522 4 also show anomalously higher cloud cover than Type 2 and Type 3 when compared to the
523 September-November climatology. This, along with the anomalous increases in RH and soil water,
524 suggests that the likelihood of precipitation is higher in Type 1 and Type 4 than in Type 2 and
525 Type 3. For Type 1 and Type 4 events, the process of dust emission and associated dust events are
526 less likely to be widespread across the Central Valley. For example, dust events could be linked to
527 the frontal passage of convective systems, where wind speeds facilitate dust emission, especially
528 when the soil is dry, particularly in the San Joaquin Valley (Pauley et al., 1996).

529

530 **3.4.2 Examples of the dominant synoptic-scale patterns.**

531 To further illustrate the two predominant patterns of synoptic-scale configurations for dust events,
532 we consider the two case studies: October 11, 2021, and November 11, 2024, dust events (Fig. 9).
533 While the October 11 case is more representative of Type 2 and Type 3 with a largely (neutrally
534 to) positively tilted trough, the November 11 case is more representative of Type 1 and Type 4
535 with a predominantly negatively (to neutrally) tilted trough (Fig. 9).

536 For the October 11, 2021, case (Fig. 9a), our results show that the positively tilted 500-mb
537 geopotential height propagates westward from 05:00 LT, when the low-pressure center is directly
538 north of California, to 14:00 LT, when the low-pressure center intensifies and moves over
539 neighboring Nevada. This intensification causes the tilt of the trough to change significantly,
540 roughly transitioning from a synoptic configuration similar to Type 2 at 05:00 LT to Type 3 by
541 11:00 LT (compare Fig. 9 and Fig. 7). Additionally, like Type 2, strong winds (greater than 6 m/s)
542 first concentrate in the Sacramento Valley. As the low-pressure center moves eastward and
543 pressure gradients over California strengthen, these strong winds expand to cover the entire Central
544 Valley, leading to widespread dust emission (see Fig. S2), aided by the dry soil and atmospheric
545 conditions (Fig. S9). Stations recorded strong winds as the event propagated southward, along with
546 a significant reduction in visibility and relative humidity (Fig. 3).

547 In contrast, for the November 11, 2024, case (Fig. 9b), the result shows a negatively tilted 500-mb
548 geopotential height, with the low-pressure center offshore over the Pacific Ocean before 10:00 LT

549 and propagating eastward over the Pacific Northwest by 19:00 LT. Additionally, a precipitation
550 band accompanies this synoptic configuration and moves southward at a similar timescale to the
551 upper-level system (Fig. S3). This synoptic-scale pattern, with associated precipitation and cloud
552 distribution over California and the Central Valley, exhibits all the characteristics of Type 1 and
553 Type 4 described above (Fig. 9 and Fig. 7). Unlike the October 11 case, which featured clear skies
554 and widespread dust emission, the November 11 event appears to be triggered by the cold pool or
555 gust fronts at the precipitation boundary and detected by the meteorological stations (see Fig. 1b
556 & Fig. 3b) coincident with dry soils (Fig. S9).

557 **3.5 Relationships between fall dust events and drought**

558 While synoptic-scale systems drive dust events in California, drought severity can modulate how
559 readily those systems produce dust by preconditioning the land surface (Achakulwisut et al., 2017).
560 By separating dust events into different drought categories, we find that most dust events occur
561 during abnormally dry to drought conditions, accounting for about 56% of dust events regardless
562 of the season (Fig. 10a). The mean precipitation onset date (i.e., the first significant rainfall event
563 across the Central Valley) shows a clear north-south gradient, with earlier onset in the northern
564 Central Valley and later onset in the southern San Joaquin Valley (Fig. S10). Consistent with this
565 pattern, the fall dust events were most frequent when the onset of precipitation was late, and
566 drought conditions were normal-dry, with such conditions accounting for the largest fraction of
567 SON dust events (35%, Fig. S11). However, a substantial fraction of SON dust events occurs in
568 early-onset years under abnormally dry (17%) and normal-dry (15%) conditions (Fig. S11).

569
570 Furthermore, to link the September-November synoptic types to hydroclimate variability, we
571 group dust events by SPEI drought category and compute the type composition (Fig. 10b). The
572 synoptic-scale configurations as drought categories show that Type 1 and Type 4 occur more
573 frequently during no-drought (63%) and normal-dry (70%) conditions than in abnormally dry
574 (33%) or drought (45%) conditions. In addition, the percentage contribution of Type 2 and Type
575 3 collectively increases from no-drought (37%) and normal-dry (30%) conditions compared to
576 abnormally dry (67%) and drought (55%) conditions. This relationship between drought categories
577 and the synoptic-scale configuration is consistent with the earlier SOM results (Fig. 7-8).
578 Specifically, Type 1 and Type 4, which occur more during no-drought and normal-dry conditions,
579 are associated with higher relative humidity and cloud cover and have a higher chance of
580 precipitation than Type 2 and Type 3, which occur more during abnormally dry and drought
581 conditions. Overall, these findings suggest that drought state and the timing of precipitation
582 modulate dust likelihood by setting land-surface susceptibility, while the dominant synoptic
583 circulation types identified (Fig. 7a) govern the wind flow that transports dust in the Central
584 Valley.

585 586 **4.0 Discussion and Conclusions**

587 This study provides a first known effort to characterize the climatology and synoptic drivers of
588 dust events in California's Central Valley. First, our analysis indicated that dust is more frequent

589 in the southern valley and has increased by about $4.4 \pm 1.5\%$ yr⁻¹ over the past two decades (2005-
590 2024). In addition, Central Valley dust events exhibit a bimodal seasonal pattern, a dominant fall
591 peak (September-November) and secondary spring peak (April to May), partly attributed to local
592 surface desiccation following the cessation of the growing season for annuals (e.g., post-harvest
593 activities and lack of irrigation) and harvest season for perennials. For example, tomato harvest
594 and processing typically span early July through October in the Central Valley (USDA NASS,
595 2024), and field operations during this period may disturb soils and increase exposed, erodible
596 surfaces. Similar disturbances occur during almond harvest, which typically begins from August
597 through October, and involves mechanical tree shaking followed by sweeping and pickup
598 operations that generate substantial PM₁₀ emissions in the San Joaquin Valley (Faulkner, 2013).
599 Furthermore, the strong bimodal seasonal pattern of dust events in the Central Valley with a fall
600 maximum contrasts with the unimodal pattern of dust from desert sources of the western United
601 States, which typically peaks in the spring (Hand et al., 2017).

602
603 Second, dust events in the Central Valley tend to peak during the late afternoon and early evening
604 hours, consistent with the diurnal maximum in boundary-layer mixing and near-surface wind
605 variability, mirroring similar patterns in neighboring dust-prone regions (Raman et al., 2014;
606 Sandhu et al., 2024). This timing also implies potential compounding with commute hours, which
607 is notable given that dust events frequently reduce visibility below 10 km (Ashley et al., 2015;
608 Vimal et al., 2019). Furthermore, more cases of valley fever are occurring in California's Central
609 Valley, particularly in the Southern San Joaquin Valley (Cooksey, 2020), where our results show
610 that dust events are more common. *Coccidioides* fungi thrive in dry soils and can be easily
611 aerosolized during typical dust events, increasing the risk of exposure, especially among farm
612 workers (McCurdy et al., 2018). Coupled with the increase in dust events over the past two decades
613 (2005-2024), this trend poses additional public health concerns.

614 Third, we demonstrate that dust events in the Central Valley are consistently associated with
615 synoptic configurations characterized by pronounced pressure gradients, which influence wind
616 directions and lead to notable differences in dust transport pathways. When the resulting flow is
617 aligned with the Central Valley axis, dust can be sustained and redistributed along the valley,
618 increasing the potential for widespread exposure and visibility hazards along major population and
619 transportation corridors, as evident in prior high-impact dust storms in the region during the 20th
620 century (e.g., Pauley et al., 1996). Among these widespread pathways, the two predominant
621 patterns characterized by eastward low-level flow closely follow synoptic patterns that produce
622 eastward winds, which carry dust from the Central Valley toward the Sierra Nevada. The eastward
623 transport of dust through this synoptic pattern can have significant implications for the Sierra
624 Nevada snowpack for winter dust events. Studies have shown that dust deposition in Sierra
625 snowpack significantly reduces albedo and radiative forcing, accelerating snowmelt timing and
626 altering runoff timing and water availability (Huang et al., 2022).

627 While dust in the Central Valley follows a particular synoptic-scale pattern, land use and surface
628 conditions, especially agricultural practices, control its sources. A significant proportion of the

629 valley plain is cultivated agricultural land. However, due to a combination of drought and long-
630 term declines of groundwater, portions of the Valley have been left fallow, potentially increasing
631 soil surface erodibility. A recent study revealed that about 77% of these fallowed agricultural lands
632 in California are in the San Joaquin Valley (Adebiyi et al., 2025) and thus provide potential
633 environments for dust emissions even under moderate wind conditions. In addition, disturbed
634 surfaces such as construction sites, unpaved roads, and dry lakebeds could serve as dust sources in
635 the valley. Drought and land use change are tightly coupled with dust emissions (Tegen et al.,
636 2004; Aryal & Evans, 2021), and an intensification of this coupled system in the region can reduce
637 available soil moisture and potentially expose the soil surface. In addition, broader future
638 projections for the southwestern US (including the Central Valley) under a warming climate
639 indicate drier conditions, which could increase the likelihood of dust events (Pu & Ginoux, 2017).

640 Despite the potential direct impacts that dust events have on human health and transportation,
641 advisories and warnings for dust impacts are quite rare in the Central Valley. For example, the
642 NWS offices in the Central Valley sparingly issued advisories or warnings for dust during the 20-
643 year period of our study, suggesting that such hazards are not well codified from a forecasting
644 perspective. This highlights the value of translating the catalog dust events information compiled
645 here into a transferable warning framework that can support NWS operations. Specifically, the
646 meteorological characteristics and synoptic patterns that modulate dust events identified in this
647 study will provide actionable inputs for a simple dust-risk indicator that could help forecasters and
648 end users anticipate periods of reduced visibility and elevated particulate exposure. We find that
649 preferred large-scale meteorological patterns coincident with dry soils are key for widespread dust
650 events. Forecasting efforts based on pattern recognition, along with more sophisticated measures
651 (Sarafian et al., 2023), may aid in the development of early warning systems for dust events that
652 can allow vulnerable populations to take protective measures and mitigate against reducing traffic
653 accidents.

654 While this study offers a comprehensive characterization of dust event dynamics across
655 California's Central Valley, we note several caveats. Our dust detection algorithm relies on
656 ASOS/AWOS data, which, despite its high temporal resolution, is subject to known observational
657 biases. These data are retrieved from a sparse network of airport stations and can sometimes miss
658 short-lived and highly localized dust, especially convective outflows that did not pass through
659 those stations. Only 11% of the dust events in our database were explicitly tagged with associated
660 dust codes (DU, BLDU, DS) by trained observers. This motivated us to expand our detection
661 through screening dusty-haze observations under dry, strong wind, and low-visibility conditions
662 to catalog dust activity that observers did not record. While this offer added value in dust detection
663 as we used a systematic approach using PM10 measurements, NWS discussions, smoke/wildfire
664 reports, and GOES satellite imagery to further codify and add an extra layer of confirmation of
665 dust events, we likely do not fully capture the scale of dust events herein. In addition, these
666 confirmatory sources have some inherent data challenges: the required PM10 temporal period
667 (2005-2024) was not available for all 15 stations; NWS discussions varied in spatial detail; and
668 satellite detection is affected by cloud cover and the timing of overpass. The reported dust event

669 presented should be interpreted as a conservative estimate, reflecting the limitations of available
670 monitoring systems in fully capturing short-lived, spatially localized, or low-intensity episodes.

671 Overall, our study significantly contributes to how regional and synoptic-scale processes interact
672 to shape dust climatology in complex agricultural basins like California's Central Valley. These
673 findings have direct implications for water resource management, air quality forecasting, public
674 health assessments, and transportation safety risk, potentially allowing communities in the Central
675 Valley to develop adaptation strategies to prepare for these events, especially as climate-driven
676 shifts in drought severity and land use continue to modulate these events.

677

678 **Acknowledgments**

679 We thank Cade Hogle for providing the wildfire and smoke event information used in screening
680 out potential smoke periods from our dust event catalog.

681 **Funding:**

682 The study was supported by the U.S. Department of Energy (DOE) Climate Resilience Center
683 (#DE-SC0024238).

684

685 **Competing interests:**

686 The authors declare that they have no competing interests

687

688 **Data availability**

689 All data used in this study are publicly available. Meteorological Aerodrome Reports (METARs)
690 obtained are available at the Iowa University Mesonet
691 (https://www.mesonet.agron.iastate.edu/request/download.phtml?network=CA_ASOS, Iowa
692 Mesonet, 2025). The ERA5 reanalysis data used is available from the Copernicus Climate Data
693 Store at <https://cds.climate.copernicus.eu/datasets> (last accessed on 08-11-2025). SPEI is obtained
694 from the National Oceanic and Atmospheric Administration (NOAA) Climate Gridded Dataset
695 (NCLimGrid) (<https://www.ncei.noaa.gov/>). We retrieve precipitation from GridMET dataset
696 (Abatzoglou, 2013; <https://www.climatologylab.org/gridmet.html>). The code and workflow data
697 used in this analysis is available for download at a Zenodo open-access repository:
698 <https://zenodo.org/records/18180271> (Precious, E. 2026)

699

700

701

702

703

704

705

706

707

708

709 **References**

710 Abatzoglou, J. T. (2013). Development of gridded surface meteorological data for ecological
711 applications and modelling [Dataset]. *International Journal of Climatology*, 33(1), 121–131.
712 <https://doi.org/10.1002/joc.3413>

713
714 Achakulwisut, P., Shen, L., & Mickley, L. J. (2017). What controls springtime fine dust variability
715 in the western United States? Investigating the 2002–2015 increase in fine dust in the US
716 Southwest. *Journal of Geophysical Research: Atmospheres*, 122(22), 12-449.

717
718 Adebisi, A. A., Kibria, M. M., Abatzoglou, J. T., Ginoux, P., Pandey, S., Heaney, A., &
719 Akinsanola, A. A. (2025). Fallowed agricultural lands dominate anthropogenic dust sources in
720 California. *Communications Earth & Environment*, 6(1), 324.

721
722 Almaraz, M., Bai, E., Wang, C., Trousdell, J., Conley, S., Faloona, I., & Houlton, B. Z. (2018).
723 Agriculture is a major source of NO_x pollution in California. *Science advances*, 4(1), eaao3477.

724
725 American Lung Association. (2025). *State of the Air 2025* (American Lung Association, 2025).

726
727 Angevine, W. M., Brioude, J., McKeen, S., Holloway, J. S., Lerner, B. M., Goldstein, A. H., ... &
728 Bon, D. (2013). Pollutant transport among California regions. *Journal of Geophysical Research:*
729 *Atmospheres*, 118(12), 6750-6763.

730
731 Ardon-Dryer, K., Gill, T. E., & Tong, D. Q. (2023). When a dust storm is not a dust storm:
732 Reliability of dust records from the storm events database and implications for geohealth
733 applications. *GeoHealth*, 7(1), e2022GH000699.

734
735 Aryal, Y. N., & Evans, S. (2021). Global dust variability explained by drought sensitivity in
736 CMIP6 models. *Journal of Geophysical Research: Earth Surface*, 126(6), e2021JF006073.

737
738 Ashley, W. S., Strader, S., Dziubla, D. C., & Haberlie, A. (2015). Driving blind: Weather-related
739 vision hazards and fatal motor vehicle crashes. *Bulletin of the American Meteorological Society*,
740 96(5), 755-778.

741
742 Bagnold, R.A. (1941). *The physics of blown sand and desert dunes*. Springer Netherlands.
743 <https://doi.org/10.1007/978-94-009-5682-7>

744
745 Ballard, M., Newcomer, M., Rudy, J., Lake, S., Sambasivam, S., Strawa, A. W., ... & Skiles, J. W.
746 (2008). Understanding the correlation of San Joaquin air quality monitoring with aerosol optical
747 thickness satellite measurements. In ASPRS Annual Conference, Baltimore MD.

748

749 Beaver, S., and A. Palazoglu, 2009: Influence of synoptic and mesoscale meteorology on ozone
750 pollution potential for San Joaquin Valley of California. *Atmos. Environ.*, 43, 1779–1788.
751

752 Benjamin, S. G., Weygandt, S. S., Brown, J. M., Hu, M., Alexander, C. R., Smirnova, T. G., ... &
753 Manikin, G. S. (2016). A North American hourly assimilation and model forecast cycle: The Rapid
754 Refresh. *Monthly Weather Review*, 144(4), 1669-1694.
755

756 Bhattachan, A., Okin, G. S., Zhang, J., Vimal, S., & Lettenmaier, D. P. (2019). Characterizing the
757 role of wind and dust in traffic accidents in California. *GeoHealth*, 3(10), 328-336.
758

759 California Department of Public Health. (2025). Valley fever in California Year-end Data
760 Dashboard. (Dashboard data last updated July 1, 2025). Retrieved 29, 2025 from
761 <https://www.cdph.ca.gov/Programs/CID/DCDC/Pages/ValleyFeverDashboard.aspx>
762

763 Cassano, J. J., E. N. Cassano, M. W. Seefeldt, W. J. Gutowski Jr., and J. M. Glisan (2016),
764 Synoptic conditions during wintertime temperature extremes in Alaska, *J. Geophys. Res. Atmos.*,
765 121, 3241–3262, doi:10.1002/2015JD024404.
766

767 Castellanos, P., Colarco, P., Espinosa, W. R., Guzewich, S. D., Levy, R. C., Miller, R. L., ... &
768 Yu, H. (2024). Mineral dust optical properties for remote sensing and global modeling: A review.
769 *Remote Sensing of Environment*, 303, 113982.
770

771 Chauhan, A., de Azevedo, S. C., & Singh, R. P. (2018). Pronounced changes in air quality,
772 atmospheric and meteorological parameters, and strong mixing of smoke associated with a dust
773 event over Bakersfield, California. *Environmental earth sciences*, 77(4), 115.
774

775 Chow, J. C., Chen, L. W. A., Watson, J. G., Lowenthal, D. H., Magliano, K. A., Turkiewicz, K.,
776 & Lehrman, D. E. (2006). PM_{2.5} chemical composition and spatiotemporal variability during the
777 California Regional PM₁₀/PM_{2.5} Air Quality Study (CRPAQS). *Journal of Geophysical*
778 *Research: Atmospheres*, 111(D10).
779

780 Chow, J. C., Watson, J. G., Lowenthal, D. H., Solomon, P. A., Magliano, K. L., Ziman, S. D., &
781 Richards, L. W. (1993). PM₁₀ and PM_{2.5} compositions in California's San Joaquin Valley.
782 *Aerosol Science and Technology*, 18(2), 105-128.
783

784 Cisneros, R., Brown, P., Cameron, L., Gaab, E., Gonzalez, M., Ramondt, S., ... & Schweizer, D.
785 (2017). Understanding public views about air quality and air pollution sources in the San Joaquin
786 Valley, California. *Journal of Environmental and Public Health*, 2017(1), 4535142.
787

788 Cook, N. J. (2023). Impact of ASOS real-time quality control on convective gust extremes in the
789 USA. *Meteorology*, 2(2), 276-294.
790

791 Cooksey, G. L. S. (2020). Regional analysis of coccidioidomycosis incidence—California, 2000–
792 2018. *MMWR. Morbidity and mortality weekly report*, 69.
793

794 David, L. M., Ravishankara, A. R., Brey, S. J., Fischer, E. V., Volckens, J., & Kreidenweis, S.
795 (2021). Could the exception become the rule? “Un-controllable” air pollution events in the U.S.
796 due to wildland fires. *Environmental Research Letters*. <https://doi.org/10.1088/1748-9326/abe1f3>
797

798 Edwards, A. (2024). Extreme dust storm halts traffic, cuts power in California’s Central Valley,
799 *San Francisco Chronicle*, 11 November. Available at:
800 <https://www.sfchronicle.com/weather/article/california-central-valley-dust-storm-19907604.php>
801

802 EPA, 2018. Current nonattainment counties for all criteria pollutants, United States Environmental
803 Protection Agency. Available at: <https://www3.epa.gov/airquality/greenbook/ancl.html> , Accessed
804 date: 2 October 2025.
805

806 Evan, A.T., Adebisi, A.A., Burney, J., Chen, S.-H., Chen, W., D’Odorico, P., Fischella, M.,
807 Heaney, A., Hoyer, K., Kok, J., Lybrand, R., Okin, G., Porter, W., Rinaldo, T., & Zender, C.S.
808 (2025, April). Beyond the haze: A UC Dust report on the causes, impacts, and future of dust storms
809 in California [Report]. UC Dust, Scripps Institution of Oceanography, University of California,
810 San Diego. [https://ucdust.ucsd.edu/wp-content/uploads/sites/492/2025/04/UC-Dust-Report-](https://ucdust.ucsd.edu/wp-content/uploads/sites/492/2025/04/UC-Dust-Report-2025.pdf)
811 [2025.pdf](https://ucdust.ucsd.edu/wp-content/uploads/sites/492/2025/04/UC-Dust-Report-2025.pdf)
812

813 Faulkner, W. B. (2013). Harvesting equipment to reduce particulate matter emissions from almond
814 harvest. *Journal of the Air & Waste Management Association*, 63(1), 70-79.
815

816 Gillette, D. A., Adams, J., Endo, A., & Smith, D. (1979). Environmental factors affecting dust
817 mobilization by wind erosion. *Saharan Dust: Mobilization, Transport, Deposition*. SCOPE Rep,
818 14, 27-48.
819

820 Ginoux, P., Prospero, J. M., Gill, T. E., Hsu, N. C., & Zhao, M. (2012). Global-scale attribution of
821 anthropogenic and natural dust sources and their emission rates based on MODIS Deep Blue
822 aerosol products. *Reviews of Geophysics*, 50(3).
823

824 Ha S, Abatzoglou JT, Adebisi A, Ghimire S, Martinez V, Wang M, et al. Impacts of heat and
825 wildfire on preterm birth. *Environ Res*. 2024;252(Pt4):119094. doi: 10.1016/j.envres.2024.119094
826

827 Hand, J. L., Gill, T. E., & Schichtel, B. A. (2017). Spatial and seasonal variability in fine mineral
828 dust and coarse aerosol mass at remote sites across the United States. *Journal of Geophysical*
829 *Research: Atmospheres*, 122(5), 3080-3097.
830

831 Hennen, M., Chappell, A., & Webb, N. P. (2023). Modelled direct causes of dust emission change
832 (2001–2020) in southwestern USA and implications for management. *Aeolian Research*, 60,
833 100852.
834

835 Hersbach, H., Bell, B., Berrisford, P., Hirahara, S., Horányi, A., Muñoz-Sabater, J., et al. (2020).
836 The ERA5 global reanalysis. *Quarterly Journal of the Royal Meteorological Society*, 146(730),
837 1999–2049. <https://doi.org/10.1002/qj.3803>
838

839 Horel, J., Splitt, M., Dunn, L., Pechmann, J., White, B., Ciliberti, C., Lazarus, S., Slemmer, J., Zaff,
840 D., & Burks, J. (2002). Mesowest: Cooperative mesonets in the western United States. *Bulletin of*
841 *the American Meteorological Society*, 83(2), 211–226.
842

843 Huang, H., Qian, Y., He, C., Bair, E. H., & Rittger, K. (2022). Snow albedo feedbacks enhance
844 snow impurity-induced radiative forcing in the Sierra Nevada. *Geophysical Research Letters*,
845 49(11), e2022GL098102.
846

847 Iowa Environmental Mesonet (2025). ASOS-AWOS-METAR Data Download,
848 https://www.mesonet.agron.iastate.edu/request/download.phtml?network=CA_ASOS
849

850 Khanum, S., Chowdhury, Z., & Sant, K. E. (2021). Association between particulate matter air
851 pollution and heart attacks in San Diego County. *Journal of the Air & Waste Management*
852 *Association*, 71(12), 1585-1594.
853

854 Klose, M., Shao, Y., Li, X., Zhang, H., Ishizuka, M., Mikami, M., & Leys, J. F. (2014). Further
855 development of a parameterization for convective turbulent dust emission and evaluation based on
856 field observations. *Journal of Geophysical Research: Atmospheres*, 119(17), 10441–10457.
857

858 Kohonen, T. (2002). The self-organizing map. *Proceedings of the IEEE*, 78(9), 1464-1480.
859

860 Kok, J. F., Parteli, E. J. R., Michaels, T. I., & Karam, D. B. (2012). The physics of wind-blown
861 sand and dust. *Reports on Progress in Physics*, 75(10), 106901.
862

863 Kolesar, K. R., Schaaf, M. D., Bannister, J. W., Schreuder, M. D., & Heilmann, M. H. (2022).
864 Characterization of potential fugitive dust emissions within the Keeler Dunes, an inland dune field
865 in the Owens Valley, California, United States. *Aeolian Research*, 54, 100765.
866

867 LaDochy, S., & Witiw, M. (2023). California Weather and Air Pollution. In Fire and Rain:
868 California's Changing Weather and Climate (pp. 185–196). Springer.
869

870 Landolt, S. D., Lave, J. S., Jacobson, D., Gaydos, A., DiVito, S., & Porter, D. (2019). The impacts
871 of automation on present weather-type observing capabilities across the conterminous United
872 States. *Journal of Applied Meteorology and Climatology*, 58(12), 2699–2715.
873

874 Leighton, P. A. (1966). Geographical aspects of air pollution. *Geographical Review*, 151–174.
875 Li, J., Wong, M. S., & Nazeer, M. (2023). Integrating physical index and self-organizing mapping
876 for aerosol dust detection (PISOM) over Himawari-8 AHI satellite images. *Atmospheric*
877 *Environment*, 309, 119921.
878

879 Luković, J., Chiang, J. C., Blagojević, D., & Sekulić, A. (2021). A later onset of the rainy season
880 in California. *Geophysical Research Letters*, 48(4), e2020GL090350.
881

882 McCurdy, S. A., Portillo-Silva, C., Sipan, C. L., Bang, H., & Emery, K. W. (2020). Risk for
883 coccidioidomycosis among Hispanic farm workers, California, USA, 2018. *Emerging Infectious*
884 *Diseases*, 26(7), 1430.
885

886 National Weather Service San Joaquin Valley/Hanford. (2024). *Storm Data and Unusual Weather*
887 *Phenomena – November 2024*. NOAA/NWS.
888

889 Neiman, P. J., Abel, M. R., Moore, B. J., Ralph, F. M., & Sukovich, E. M. (2013). Sierra barrier
890 jets, atmospheric rivers, and precipitation characteristics in Northern California: A composite
891 perspective based on a network of wind profilers. *Monthly Weather Review*, 141(12), 4211-4233.
892

893 NOAA, 1998: *Automated Surface Observing System (ASOS) user's guide*. National Weather
894 Service Doc., 38 pp., <https://www.weather.gov/media/asos/aum-toc.pdf>.
895

896 NOAA. (2025). National centers for environmental information, Climate monitoring.
897 <https://www.ncei.noaa.gov/access/monitoring/products/>, last accessed in August
898 2025.
899

900 Pauley, P. M., Baker, N. L., & Barker, E. H. (1996). An observational study of the “Interstate 5”
901 dust storm case. *Bulletin of the American Meteorological Society*, 77(4), 693-720.
902

903 Precious, E. (2026). Dataset for Characterization of Dust events over California's Central Valley
904 [Data set]. Zenodo. <https://doi.org/10.5281/zenodo.18180271>
905

906 Pu, B., & Ginoux, P. (2017). Projection of American dustiness in the late 21st century due to
907 climate change. *Scientific Reports*, 7(1), 5553.
908

909 Raman, A., Arellano, A. F., & Brost, J. J. (2014). Revisiting haboobs in the southwestern United
910 States: An observational case study of the 5 July 2011 Phoenix dust storm. *Atmospheric*
911 *Environment*, 89, 179–188. <https://doi.org/10.1016/J.ATMOSENV.2014.02.026>
912

913 Robinson, M. C., & Ardon-Dryer, K. (2024). Characterization of 21 years of dust events across
914 four West Texas regions. *Aeolian Research*, 67, 100930.
915

916 Rowan, C., D’Souza, R. R., Zheng, X., Crooks, J., Hohsfield, K., Tong, D., Chang, H. H., & Ebel,
917 S. (2024). Dust storms and cardiorespiratory emergency department visits in three Southwestern
918 United States: application of a monitoring-based exposure metric. *Environmental Research:*
919 *Health*, 2(3), 031003.
920

921 San Joaquin Valley Air Pollution Control District. Ambient air quality standards and Valley
922 attainment status. Retrieved August 23, 2025, from [https://www.valleyair.org/air-quality-](https://www.valleyair.org/air-quality-information/ambient-air-quality-standards-valley-attainmnet-status/)
923 [information/ambient-air-quality-standards-valley-attainmnet-status/](https://www.valleyair.org/air-quality-information/ambient-air-quality-standards-valley-attainmnet-status/)
924

925 Sandhu, T., Kelley, M., Rawlins, E., & Ardon-Dryer, K. (2024). Identification of dust events in
926 the greater Phoenix area. *Atmospheric Pollution Research*, 15(11), 102275.
927 <https://doi.org/10.1016/j.apr.2024.102275>
928

929 Sarafian, R., Nissenbaum, D., Raveh-Rubin, S., Agrawal, V., & Rudich, Y. (2023). Deep multi-
930 task learning for early warnings of dust events implemented for the Middle East. *NPJ climate and*
931 *atmospheric science*, 6(1), 23.
932

933 Shao, Y. (Ed.). (2008). *Physics and modelling of wind erosion*. Dordrecht: Springer Netherlands.
934

935 Sheridan, S. C., & Lee, C. C. (2011). The self-organizing map in synoptic climatological research.
936 *Progress in Physical Geography*, 35(1), 109-119.
937

938 Suarez-Molina, D., Cuevas, E., Alonso-Pérez, S., Cana, L., Montero, G., & Oliver, A. (2024). Dust
939 events characterization from visibility, trends, and Dust Adversity Index in the Canary Islands for
940 1980–2022. *Heliyon*, 10(10).
941

942 Sweeney, A., Loikith, P., & Lintner, B. (2017). Characterizing Large-Scale Meteorological
943 Patterns and Associated Temperature and Precipitation Extremes over the Northwestern United
944 States Using Self-Organizing Maps. *Journal of Climate*, 30, 2829-2847.
945 <https://doi.org/10.1175/JCLI-D-16-0670.1>.
946

947 Taylor, G. P., Loikith, P. C., Lee, H. K., Rahimi, S., & Hall, A. (2025). Historical and future
948 autumn rain and wind onset over western North America using regional climate models. *Journal*
949 *of Geophysical Research: Atmospheres*, 130(21), e2025JD044267.
950

951 Tegen, I., Werner, M., Harrison, S. P., & Kohfeld, K. E. (2004). Relative importance of climate
952 and land use in determining present and future global soil dust emission. *Geophysical Research*
953 *Letters*, 31(5).
954

955 Tong, D. Q., Dan, M., Wang, T., & Lee, P. (2012). Long-term dust climatology in the western
956 United States reconstructed from routine aerosol ground monitoring. *Atmospheric Chemistry and*
957 *Physics*, 12(11), 5189–5205.

958 Tong, D. Q., Gill, T. E., Sprigg, W. A., Van Pelt, R. S., Baklanov, A. A., Barker, B. M., Bell, J.
959 E., Castillo, J., Gassó, S., & Gaston, C. J. (2023). Health and safety effects of airborne soil dust in
960 the Americas and beyond. *Reviews of Geophysics*, 61(2), e2021RG000763.
961

962 Tong, D. Q., Wang, J. X. L., Gill, T. E., Lei, H., & Wang, B. (2017). Intensified dust storm activity
963 and Valley fever infection in the southwestern United States. *Geophysical Research Letters*, 44(9),
964 4304–4312.
965

966 Uotila, P., Perkins-Kirkpatrick, S., Pepler, A., Gibson, P., & Alexander, L. (2017). On the use of
967 self-organizing maps for studying climate extremes. *Journal of Geophysical Research:*
968 *Atmospheres*, 122, 3891 - 3903. <https://doi.org/10.1002/2016JD026256>.
969

970 U.S. Department of Agriculture, National Agricultural Statistics Service. (2024, August 29). 2024
971 California processing tomato report.
972 [https://www.nass.usda.gov/Statistics_by_State/California/Publications/Specialty_and_Other_Rel](https://www.nass.usda.gov/Statistics_by_State/California/Publications/Specialty_and_Other_Rel_eases/Tomatoes/2024/202408ptom.pdf)
973 [eases/Tomatoes/2024/202408ptom.pdf](https://www.nass.usda.gov/Statistics_by_State/California/Publications/Specialty_and_Other_Rel_eases/Tomatoes/2024/202408ptom.pdf)
974

975 Vimal, S., Lettenmaier, D., Okin, G., Zhang, J., & Bhattachan, A. (2019). Characterizing the Role
976 of Wind and Dust in Traffic Accidents in California. *GeoHealth*, 3, 328 - 336.
977 <https://doi.org/10.1029/2019GH000212>.
978

979 Wang, M., & Ullrich, P. (2018). Marine air penetration in California’s Central Valley:
980 Meteorological drivers and the impact of climate change. *Journal of Applied Meteorology and*
981 *Climatology*, 57(1), 137–154.
982

983 Wang, T., Zhao, B., Liou, K.-N., Gu, Y., Jiang, Z., Song, K., Su, H., Jerrett, M., & Zhu, Y. (2019).
984 Mortality burdens in California due to air pollution attributable to local and nonlocal emissions.
985 *Environment International*, 133, 105232.
986

987 WMO (World Meteorological Organization). (2019). WMO technical regulations annex II manual
988 on codes international codes. I. 1.
989

990 Wilshire, H. G., Nakata, J. K., & Hallet, B. (1981). Field observations of the December 1977 wind
991 storm, San Joaquin Valley, California.
992

993 Wittek, P., Gao, S. C., Lim, I. S., & Zhao, L. (2017). Somoclu: An efficient parallel library for
994 self-organizing maps. *Journal of Statistical Software*, 78, 1-21.
995

996 Xi, X. (2020). Global aeolian dust variations and trends: a revisit of dust event and visibility
997 observations from surface weather stations. *Atmospheric Chemistry and Physics Discussions*,
998 2020, 1–34.
999

1000 Young, B. N., Tryner, J., Hernandez Ramirez, L., WeMott, S., Erlandson, G., Li, X., Kuiper, G.,
1001 Dean, D. A., Martinez, N., & Phillips, M. (2025). Particulate Matter Pollution in an Agricultural
1002 Setting: A Community-Engaged Research Study. *Environments*, 12(10), 348.
1003

1004 Young, D. E., Kim, H., Parworth, C., Zhou, S., Zhang, X., Cappa, C. D., Seco, R., Kim, S., &
1005 Zhang, Q. (2016). Influences of emission sources and meteorology on aerosol chemistry in a
1006 polluted urban environment: results from DISCOVER-AQ California. *Atmospheric Chemistry and*
1007 *Physics*, 16(8), 5427–5451.
1008

1009 Zarate-Gonzalez, G., Brown, P., & Cisneros, R. (2024). Costs of air pollution in california’s san
1010 joaquin valley: A societal perspective of the burden of asthma on emergency departments and
1011 inpatient care. *Journal of Asthma and Allergy*, 369–382.
1012

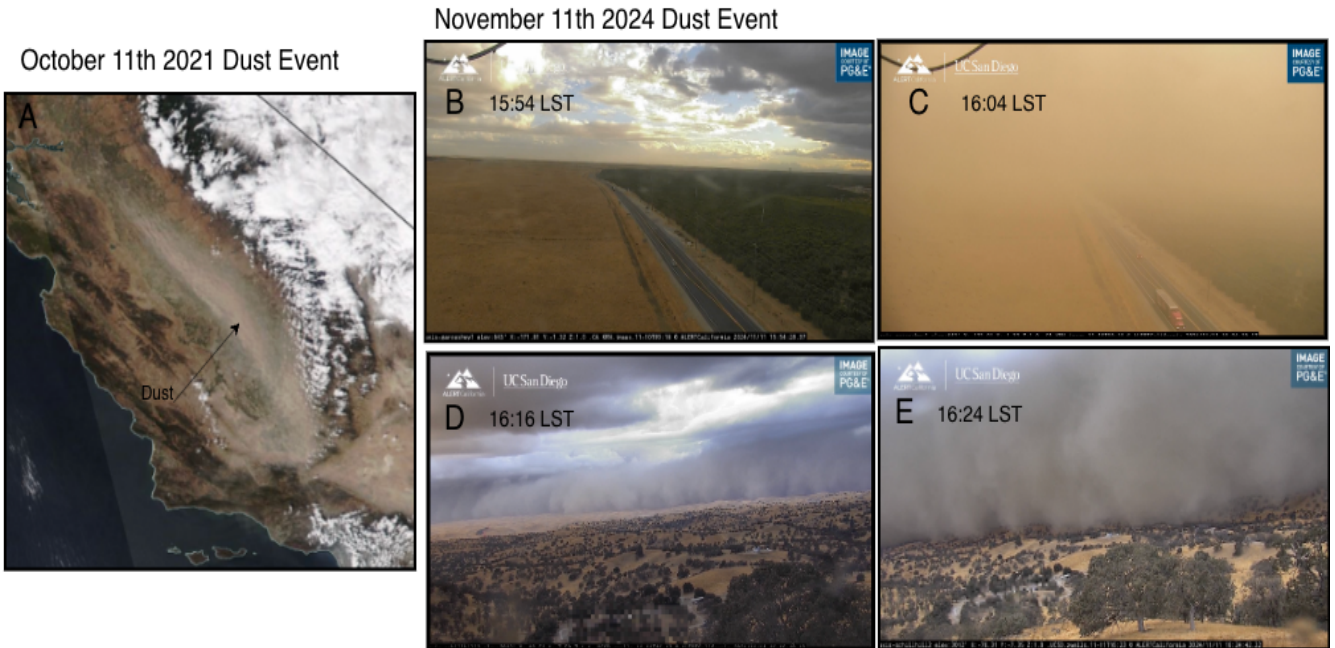
1013 Zeeshan, N., Freer-Smith, P., Murtaza, G., Wong, A. E., & Taylor, G. (2024). His dark materials:
1014 quantifying the problem of dust (particulate matter) in the agricultural landscape of California.
1015 *Atmospheric Environment*, 330, 120562.
1016

1017 Zuo, X., Zhang, C., Zhang, X., Wang, R., Zhao, J., & Li, W. (2024). Wind tunnel simulation of
1018 wind erosion and dust emission processes, and the influences of soil texture. *International Soil and*
1019 *Water Conservation Research*, 12(2), 455–466.
1020

1021 Zhao, Z., Chen, S.-H., Kleeman, M. J., Tyree, M., & Cayan, D. (2011). The impact of climate
1022 change on air quality–related meteorological conditions in California. Part I: present time
1023 simulation analysis. *Journal of Climate*, 24(13), 3344–3361.
1024
1025
1026

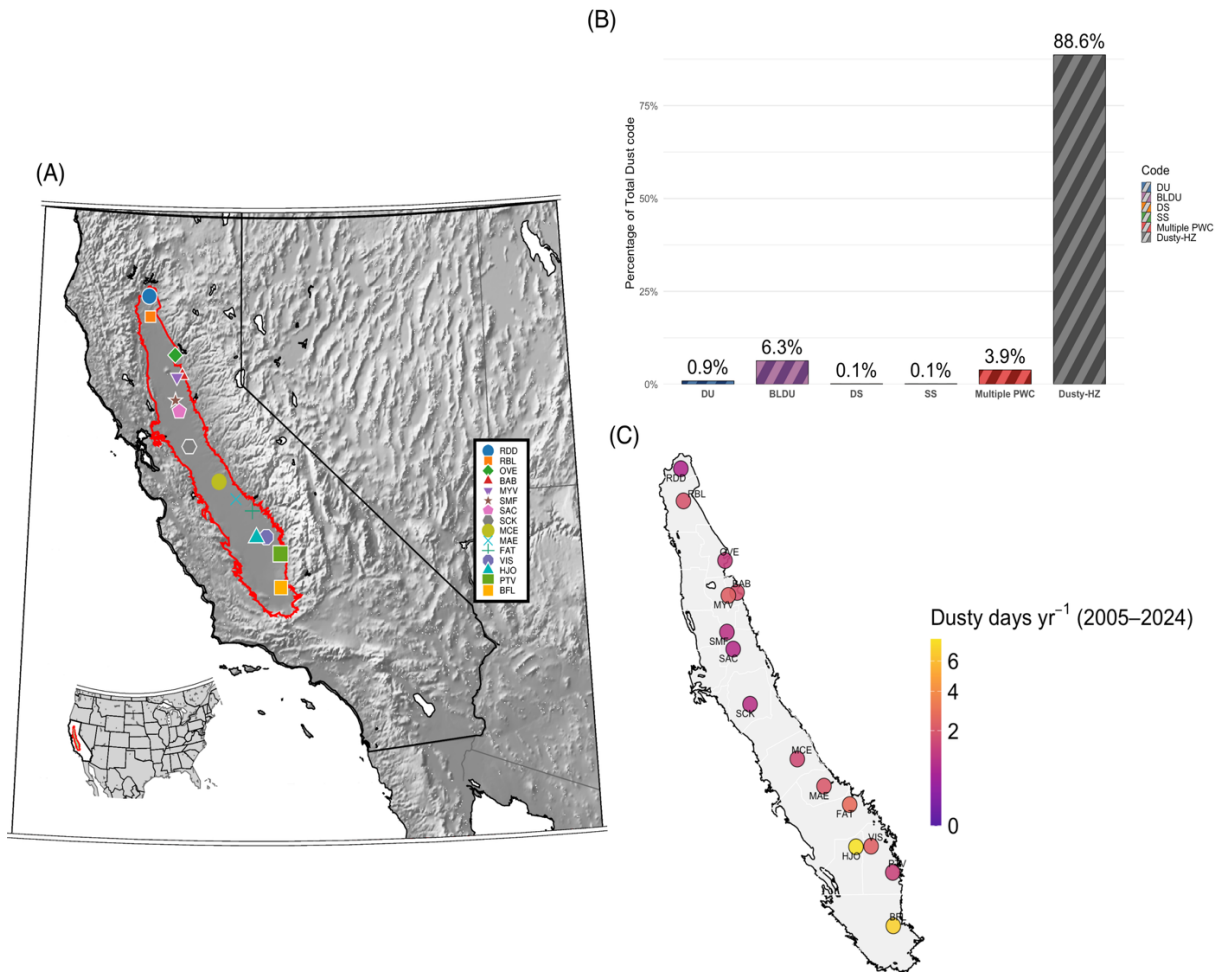
1027
1028

FIGURES



1029
1030
1031
1032
1033
1034
1035
1036
1037
1038
1039
1040
1041
1042
1043
1044

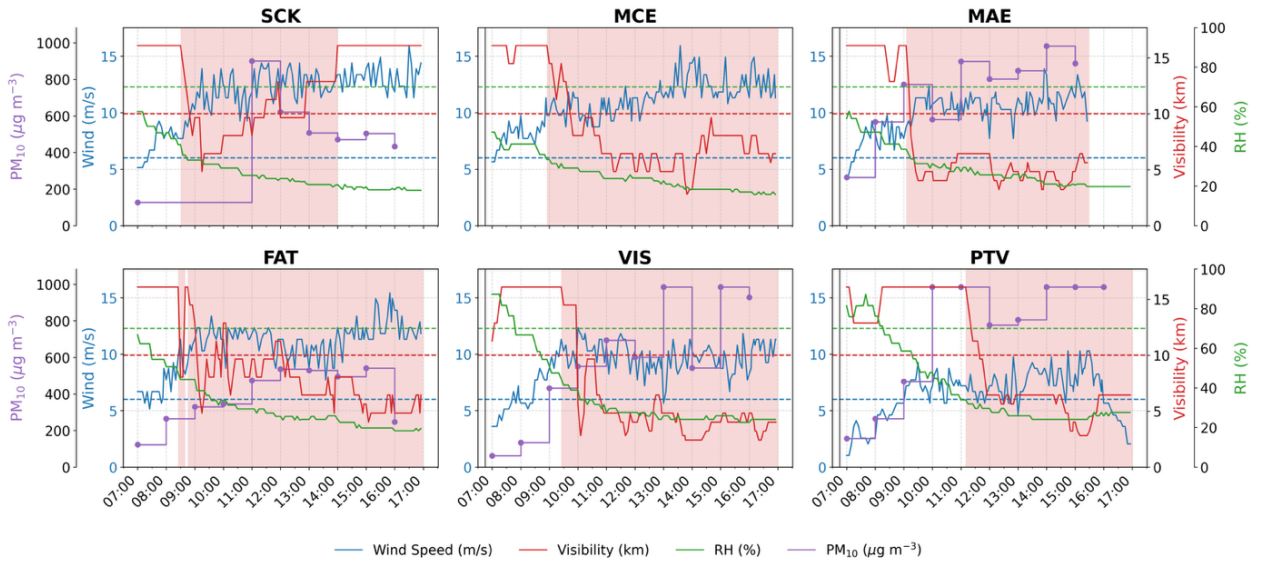
Fig 1. Satellite and ground-based view of two California Central Valley dust events. (a) The true-color satellite image for October 11, 2021, from NASA Worldview, shows a widespread along-valley dust event. (b-e) The UC San Diego ALERT California camera network (in Kern County, along Garces Highway (CA-119 corridor) west/southwest of Bakersfield (b & c) and Southern Sierra foothills/Kern River Lake Isabella area (d & e) during the November 11, 2024, haboob dust event, showing conditions before (b, d) and during (c, e) the dust passage.



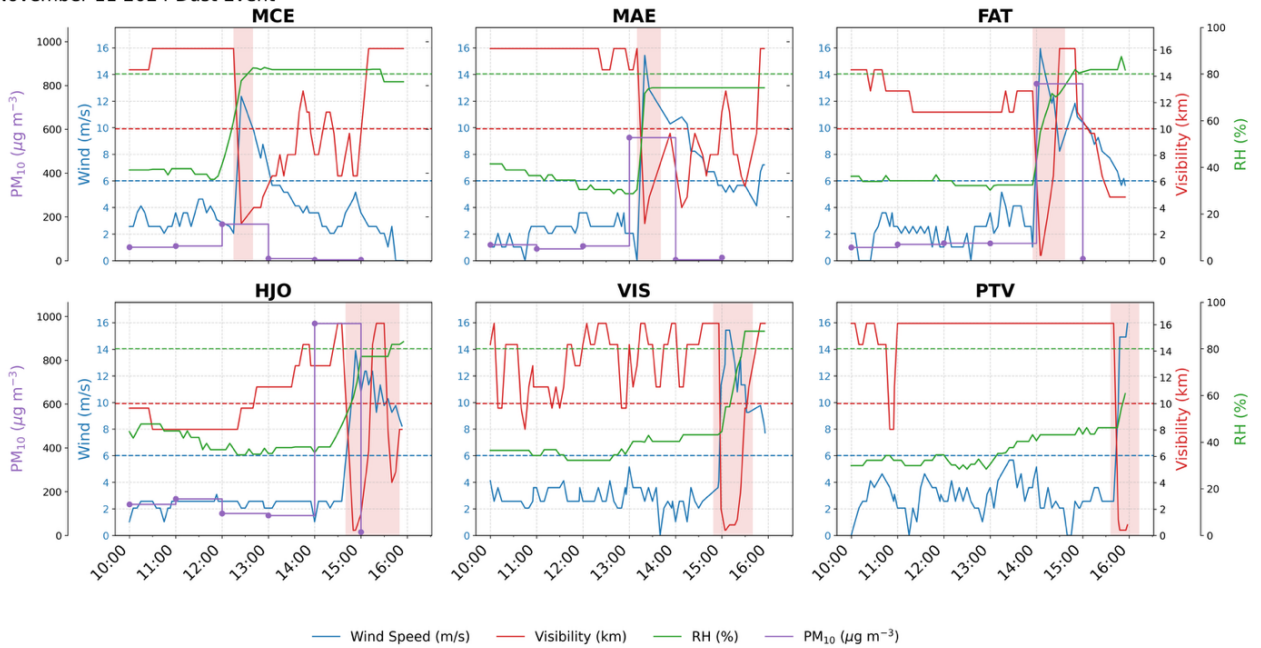
1045
 1046
 1047
 1048
 1049
 1050
 1051
 1052
 1053
 1054
 1055

Fig 2. Dust occurrence across the California Central Valley. (a) Study area map showing the Central Valley (red outline) and 15 meteorological stations (see details of the stations in Table S1) (b) Percentage fraction of dust-related present weather codes (PWC) reported across all stations from 2005-2024. Codes are DU (Widespread dust), BLDU (blowing dust), DS (dust storm), SS (sandstorm), Multiple PWC (report of more than one dust related code) and Dusty-HZ (dusty haze conditions under dry, strong windy and reduced visibility conditions) (c) 20-year annual average of station-level dusty days.

(a) October 11 2021 Dust Event



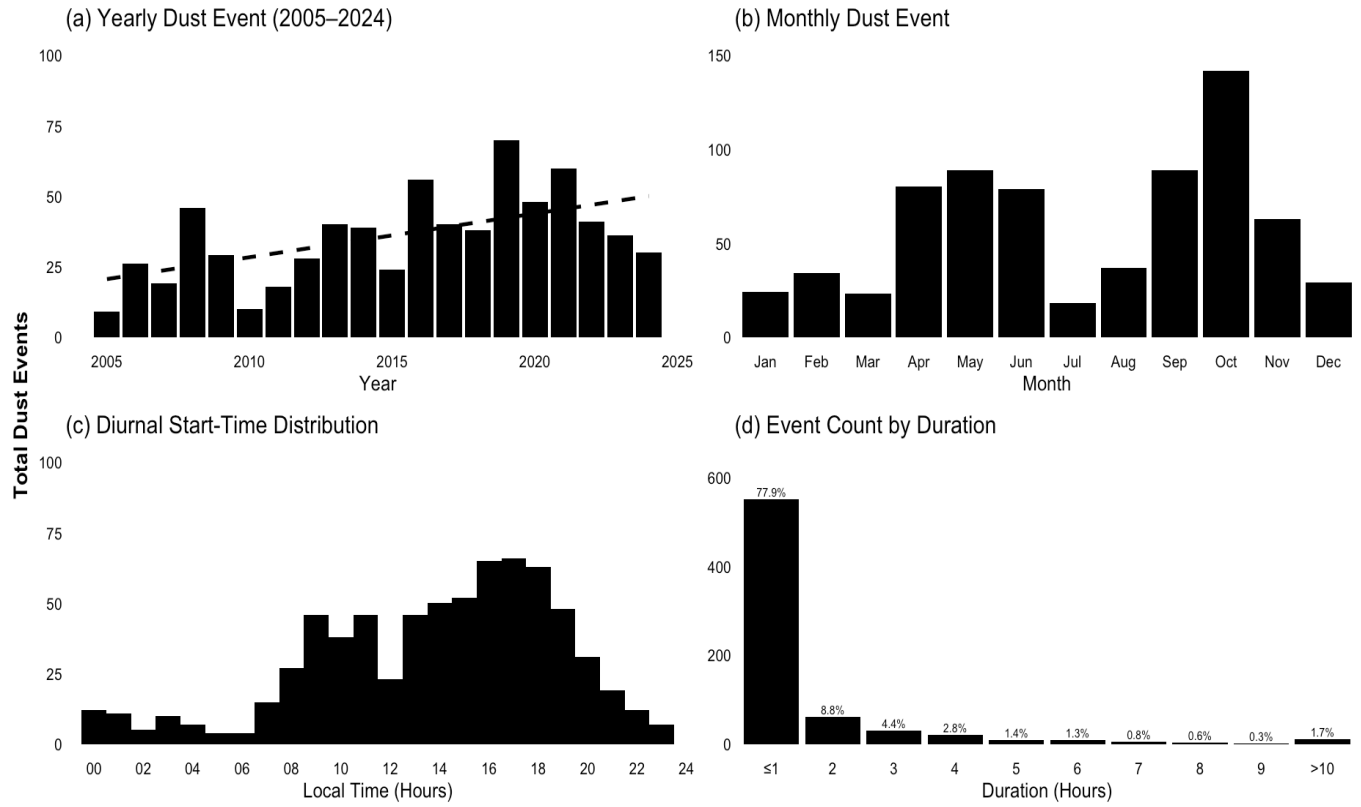
(b) November 11 2024 Dust Event



1056
1057
1058
1059
1060
1061
1062
1063
1064
1065
1066

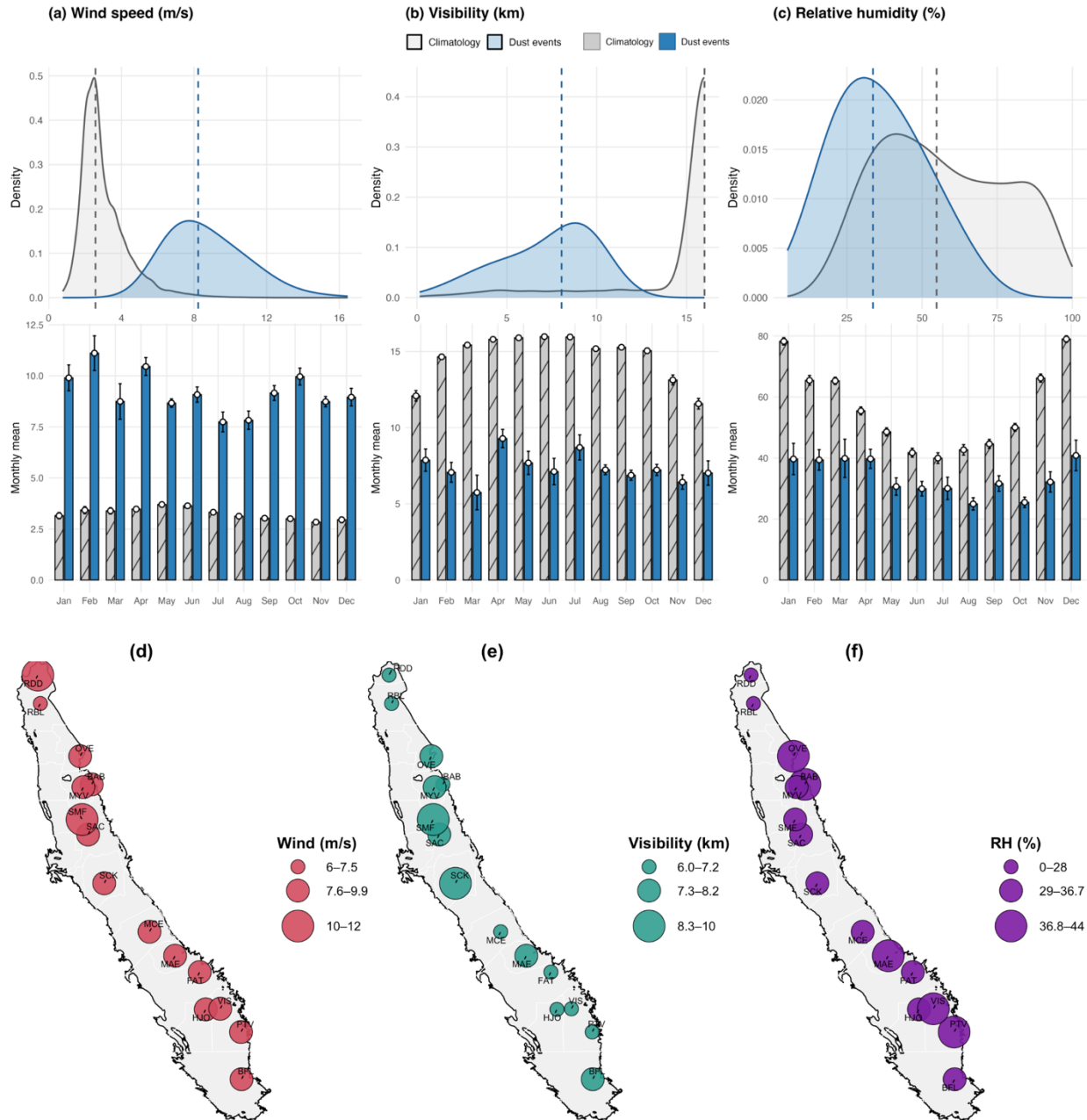
Fig 3. Wind speed (blue lines), visibility (red lines), and relative humidity (green lines) during (a) October 11, 2021, (b) November 11, 2024, at meteorological stations. Associated hourly PM₁₀ data from nearby stations are shown in purple lines. Highlighted in pink are dust events meeting the criteria described in section 2.2, with dashed horizontal lines showing thresholds of wind speed, visibility, and relative humidity used.

1067
1068



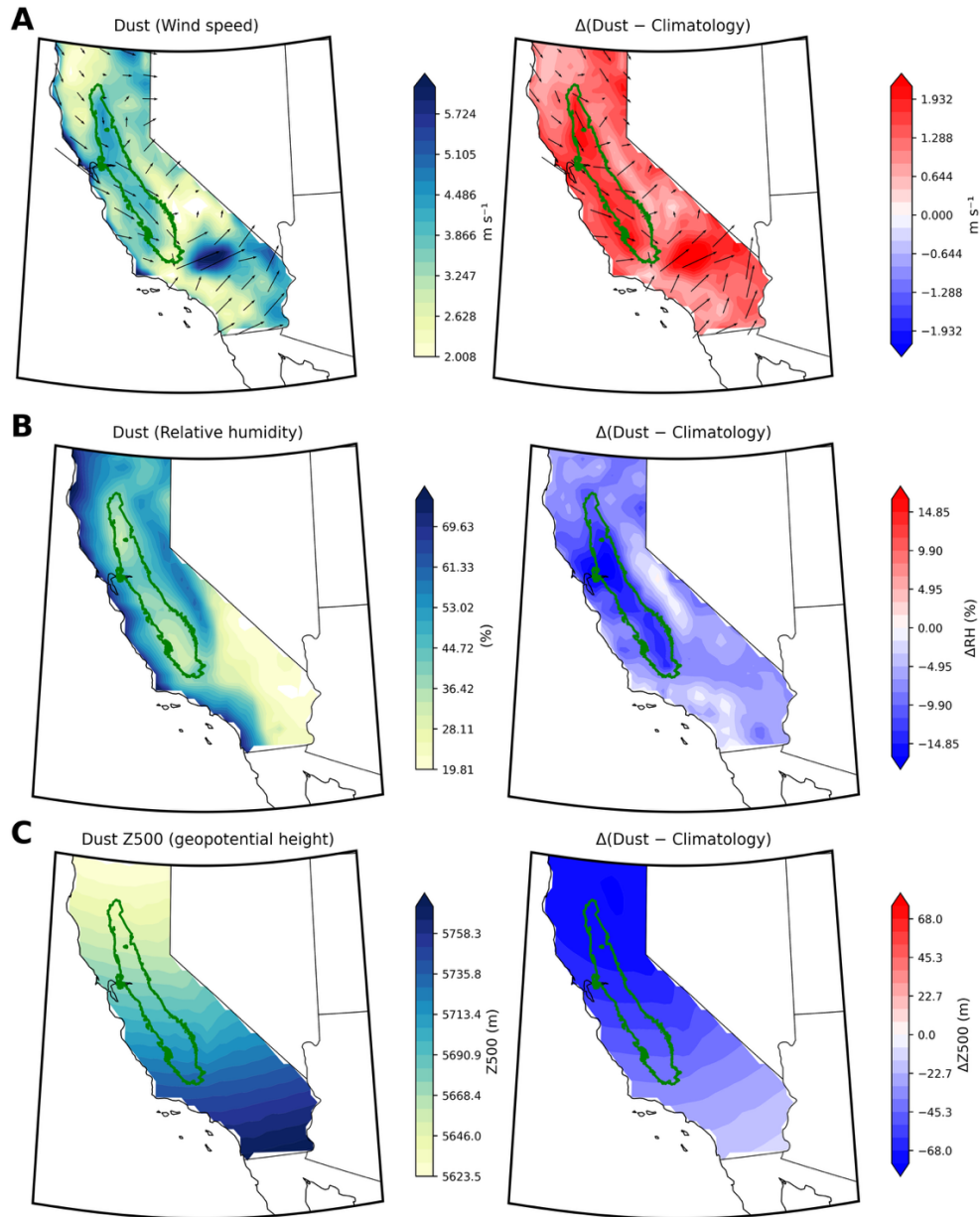
1069
1070
1071
1072
1073
1074
1075

Fig 4. Temporal distribution of dust events in the Central Valley for 2005–2024. (a) Yearly distribution, (b) monthly distribution, (c) diurnal distribution, and (d) duration of dust events.



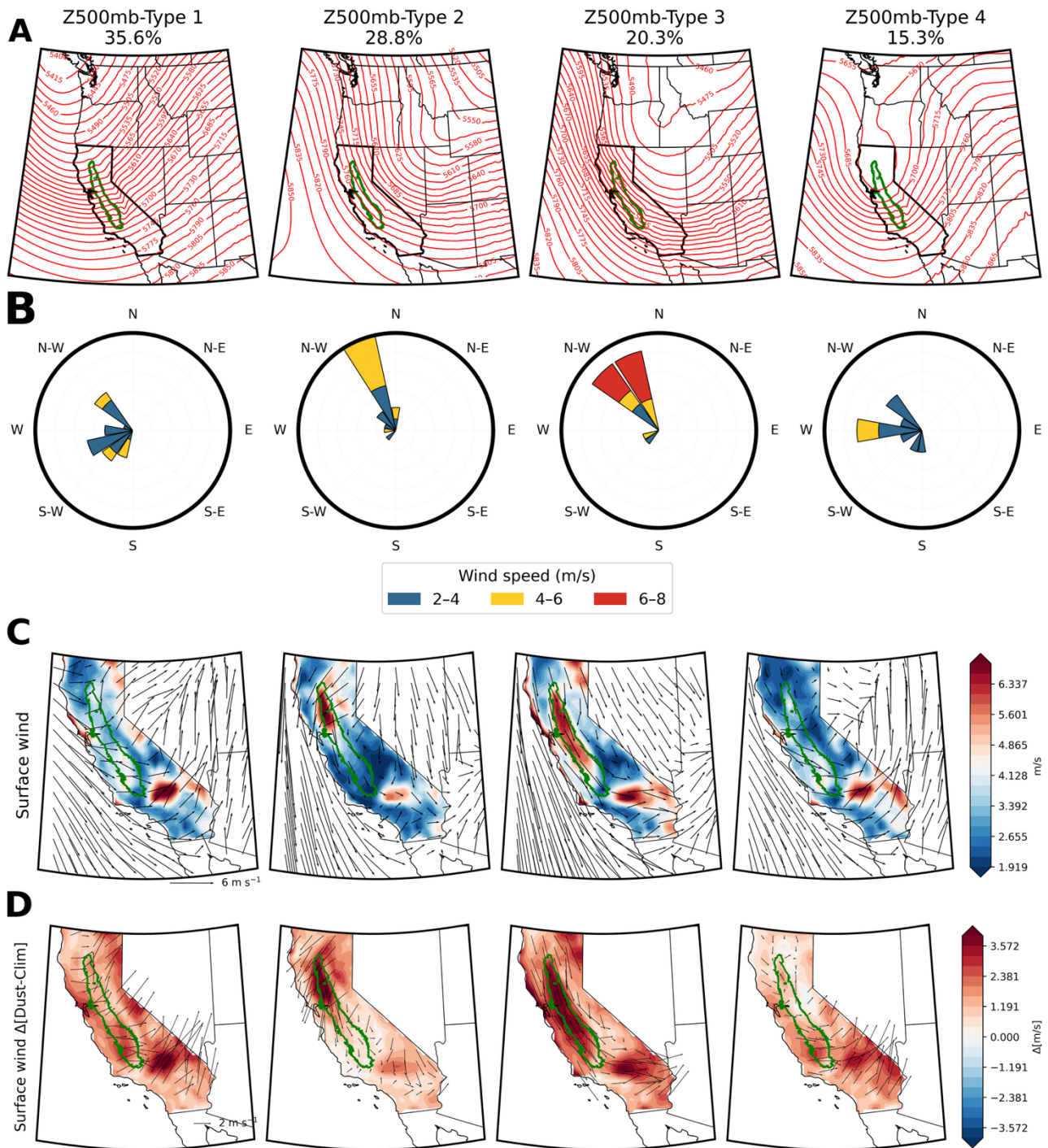
1076
 1077
 1078
 1079
 1080
 1081
 1082
 1083
 1084
 1085

Fig 5. Distributions of meteorological conditions during dust events. (a-c) Probability distributions and monthly means surface wind (m/s), visibility (km), and relative humidity (%) for the dust events (blue) compared to climatology (grey); error bars show variability across the stations. (d-f) Spatial patterns of station mean of surface wind (m/s), visibility (km), and relative humidity (%) during dust events; symbol size encodes magnitude.



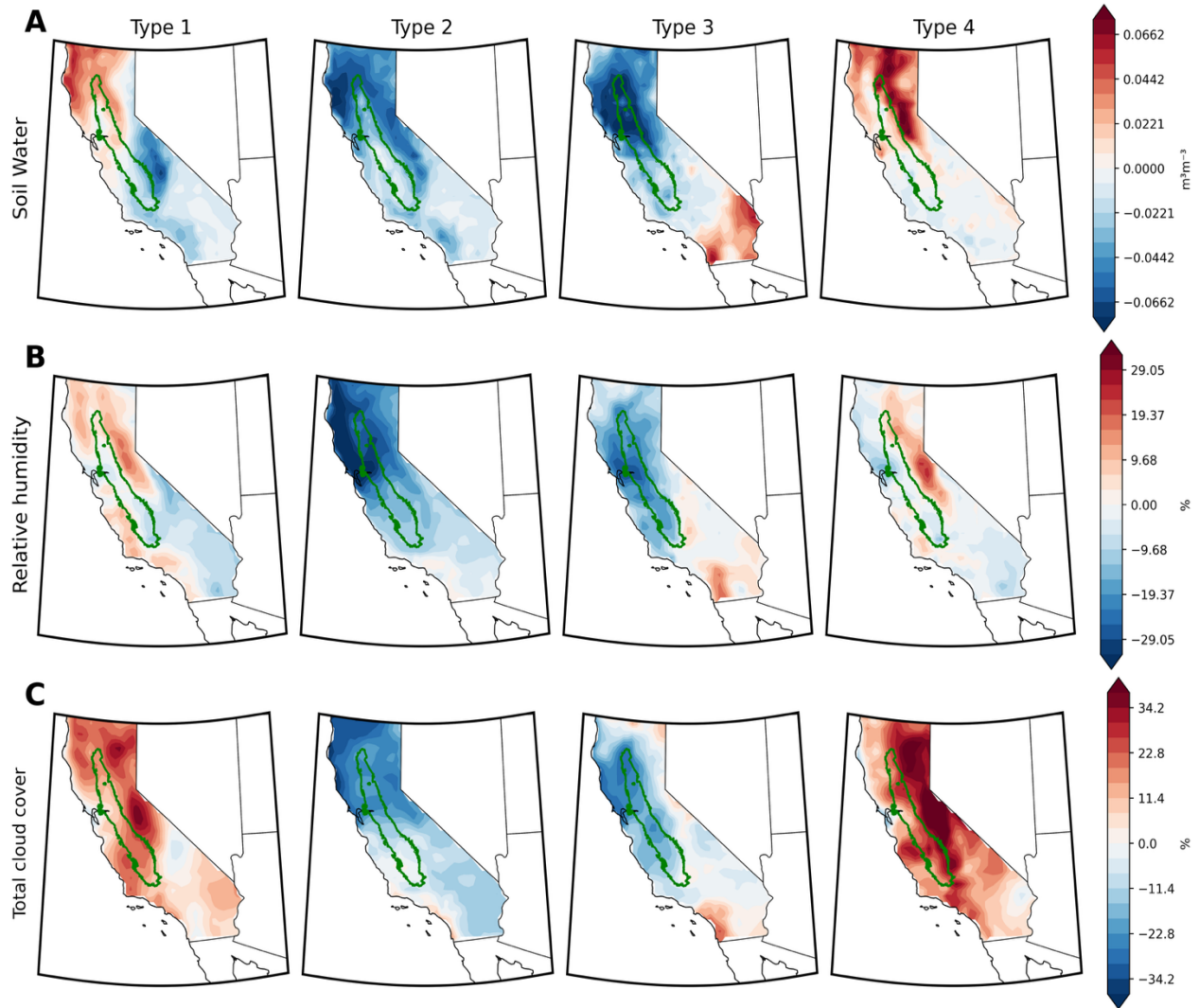
1086
 1087 **Fig 6.** Dust-event composites (left) and anomalies relative to climatology (right) from ERA5
 1088 reanalysis. Rows show: (a) 10-m wind speed (m s^{-1}) with 10-m wind vectors, (b) near-surface
 1089 relative humidity (%), (c) 500-hPa geopotential (Z500, m). The green outline denotes the Central
 1090 Valley.

1091
 1092
 1093
 1094

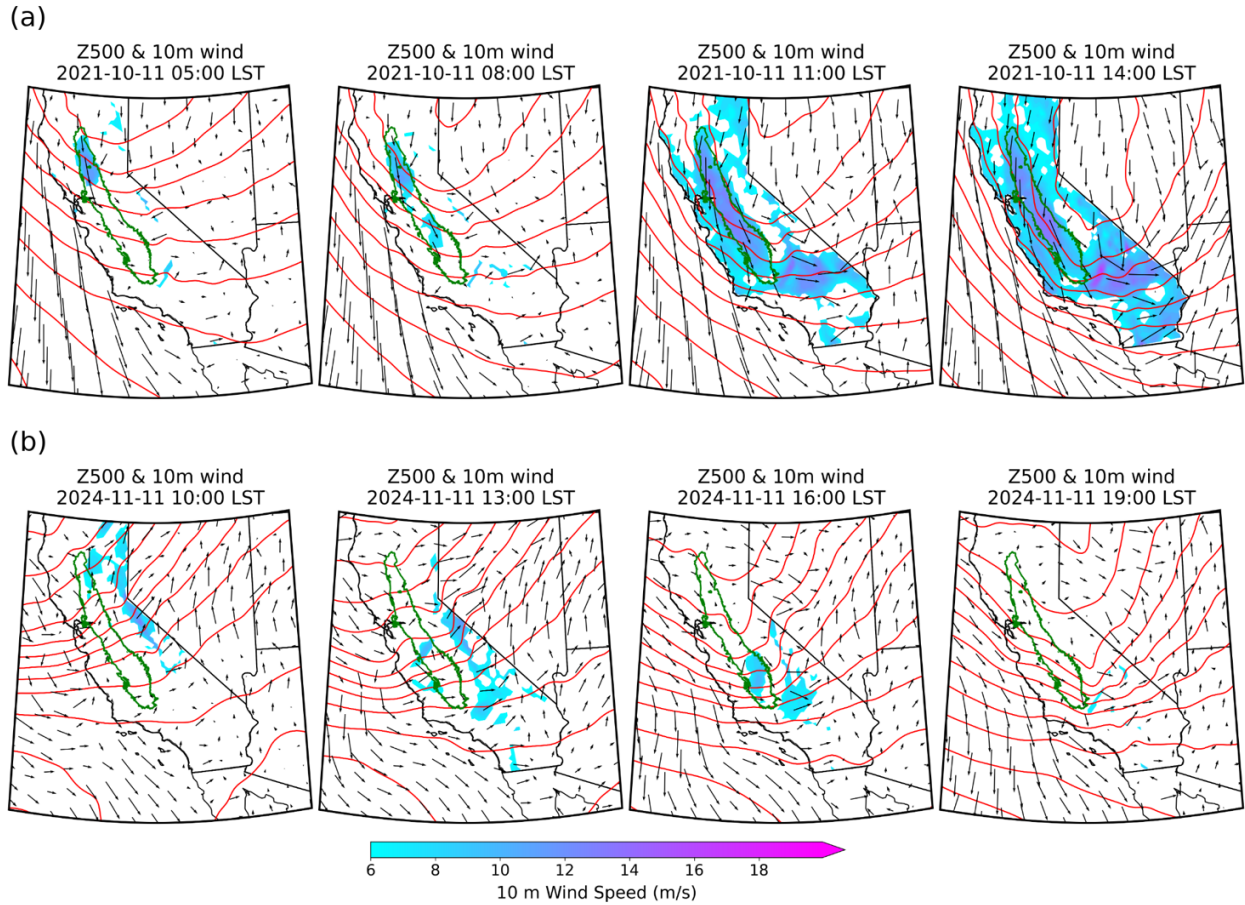


1095
 1096
 1097
 1098
 1099
 1100
 1101

Fig 7. Synoptic configuration pattern during widespread dust event in the Central Valley. (a) SOM composite of 500-hpa geopotential (m) bin into four dominant circulation types with the percentage of dusty days each type represented, (b) wind orientation and speed associated with each Type over the Central Valley, (c) Mean surface wind speed on dusty days for each Type; shading indicates wind speed (m/s) and arrows shows vector direction; (d) surface wind anomalies relative to climatology.



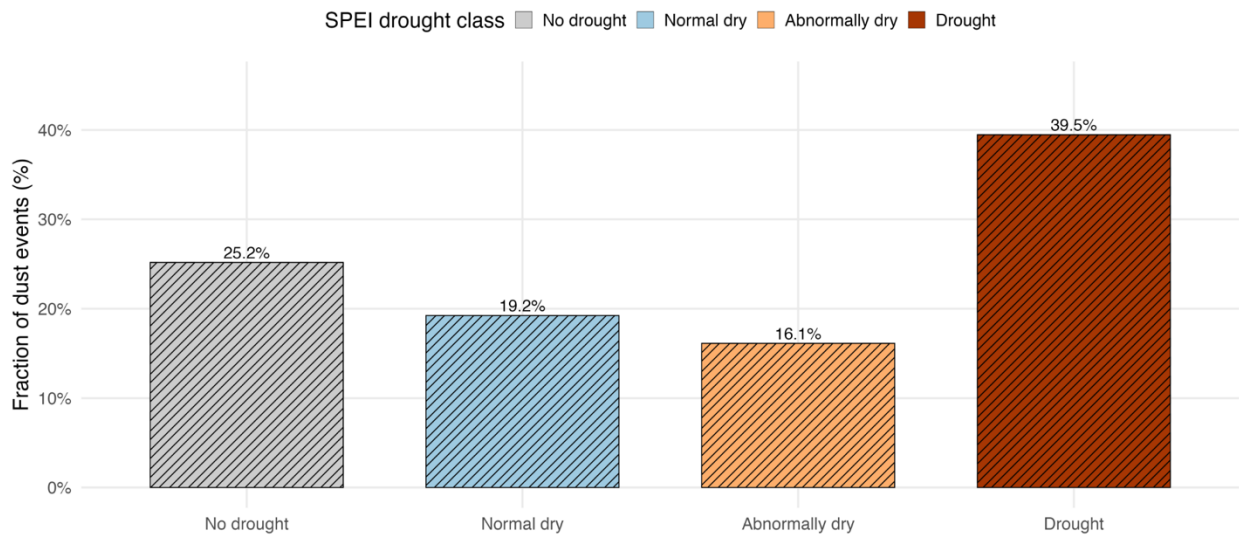
1102
 1103 **Fig 8.** Environmental variables associated with the four dominant circulation types for Central
 1104 Valley dust events (as identified in Fig 7a). Columns show Type 1 to 4; Rows show composite
 1105 anomalies relative to the climatology mean for (a) surface soil water (m^3m^{-3}), (b) relative
 1106 humidity (%), and (c) total cloud cover (%). The green outline marks the Central Valley domain.
 1107
 1108
 1109
 1110
 1111
 1112
 1113
 1114
 1115
 1116



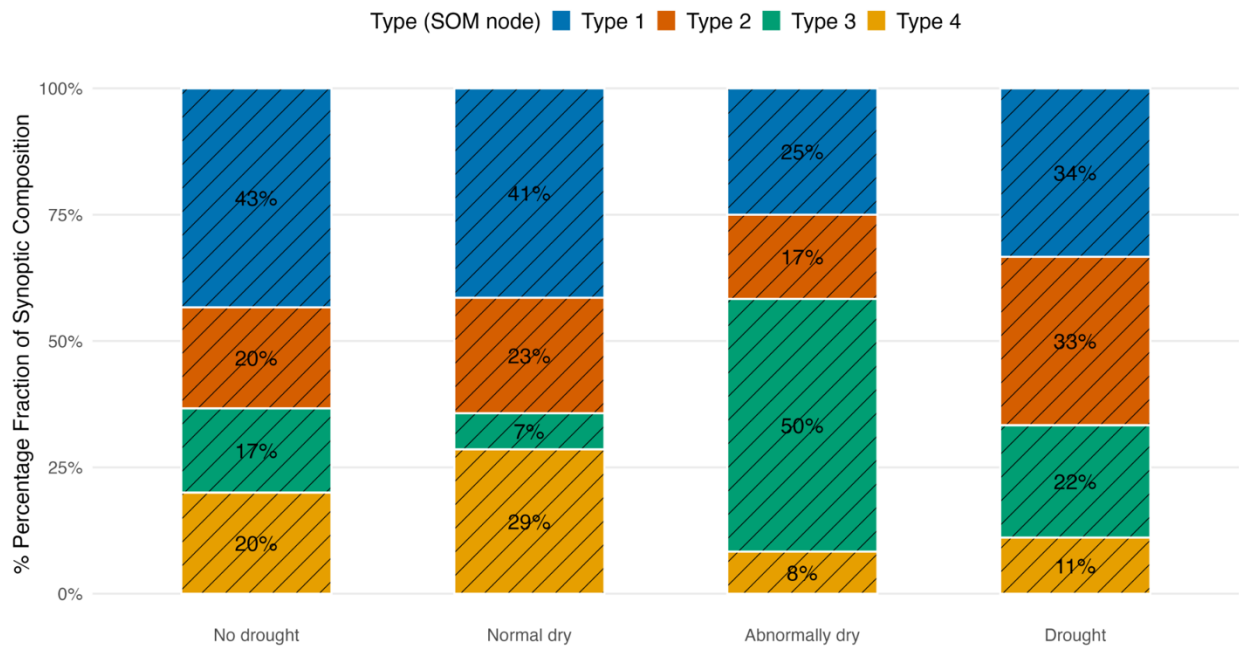
1117
1118
1119
1120
1121
1122
1123
1124

Fig 9. Temporal evolution of synoptic pattern and near-surface wind during two major Central Valley dust events. Panels show 500-hpa geopotential (m ; red contours), surface wind vectors (black arrows), and surface wind speed (shading $> 6\text{ m/s}$) during October 11, 2021 (top) and November 11, 2024 (bottom) from the RAPv3 dataset. The green outline marks the Central Valley domain.

(a).



(b).



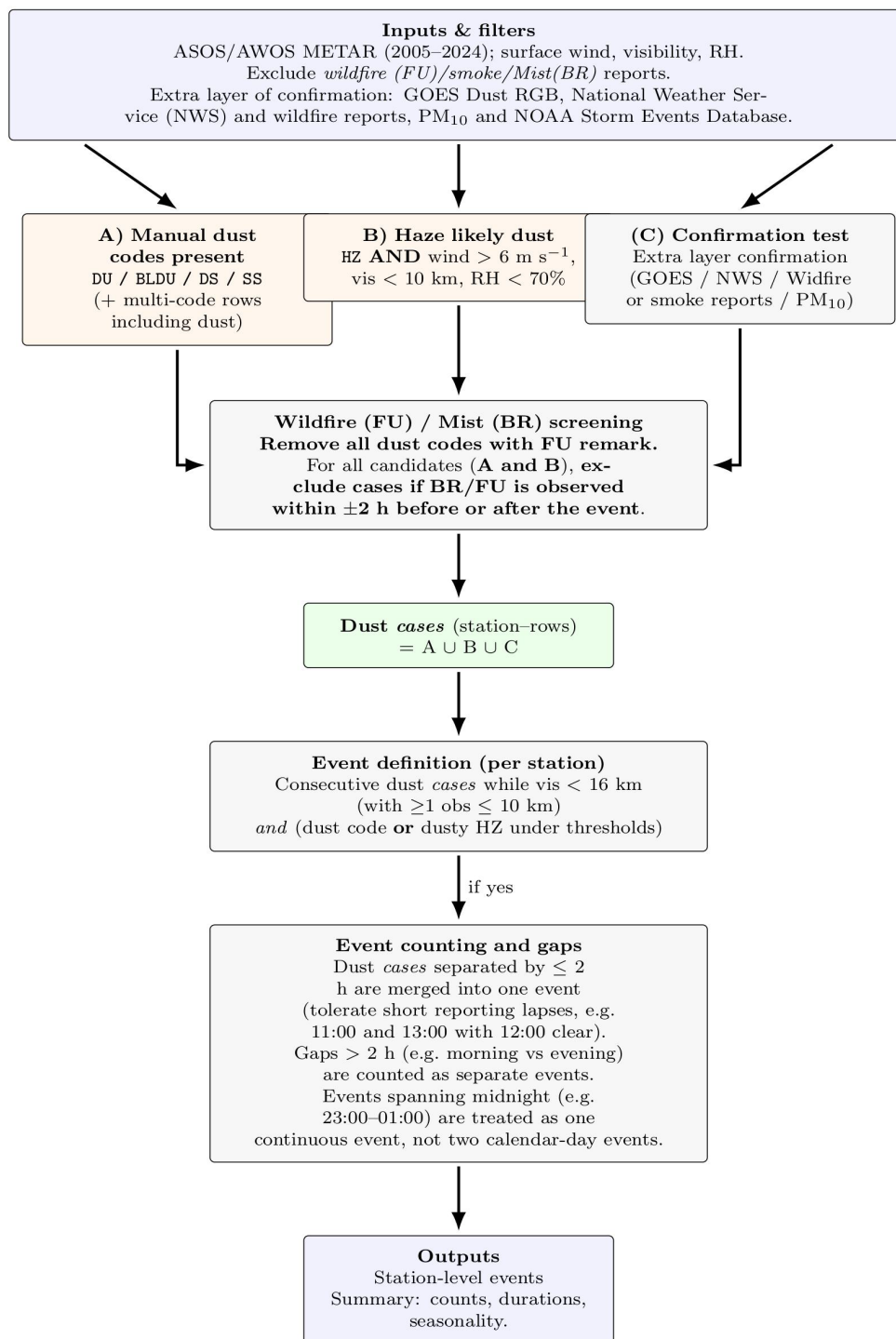
1125
1126
1127
1128
1129
1130
1131
1132
1133

Fig 10. (a) Percentage fraction of dust events as a function of SPEI categories (2005-2024) and (b) distribution of synoptic configurations (as identified in Fig 7a) during dust events across drought. Stacked bars show the percentage fraction of dust events associated with each synoptic configuration/Type as a function of drought severity class.

1134
1135

Supplementary

Dust-Event Detection Algorithm



1136
1137

Figure S1. Flowchart showing the procedure used for dust-event identification.

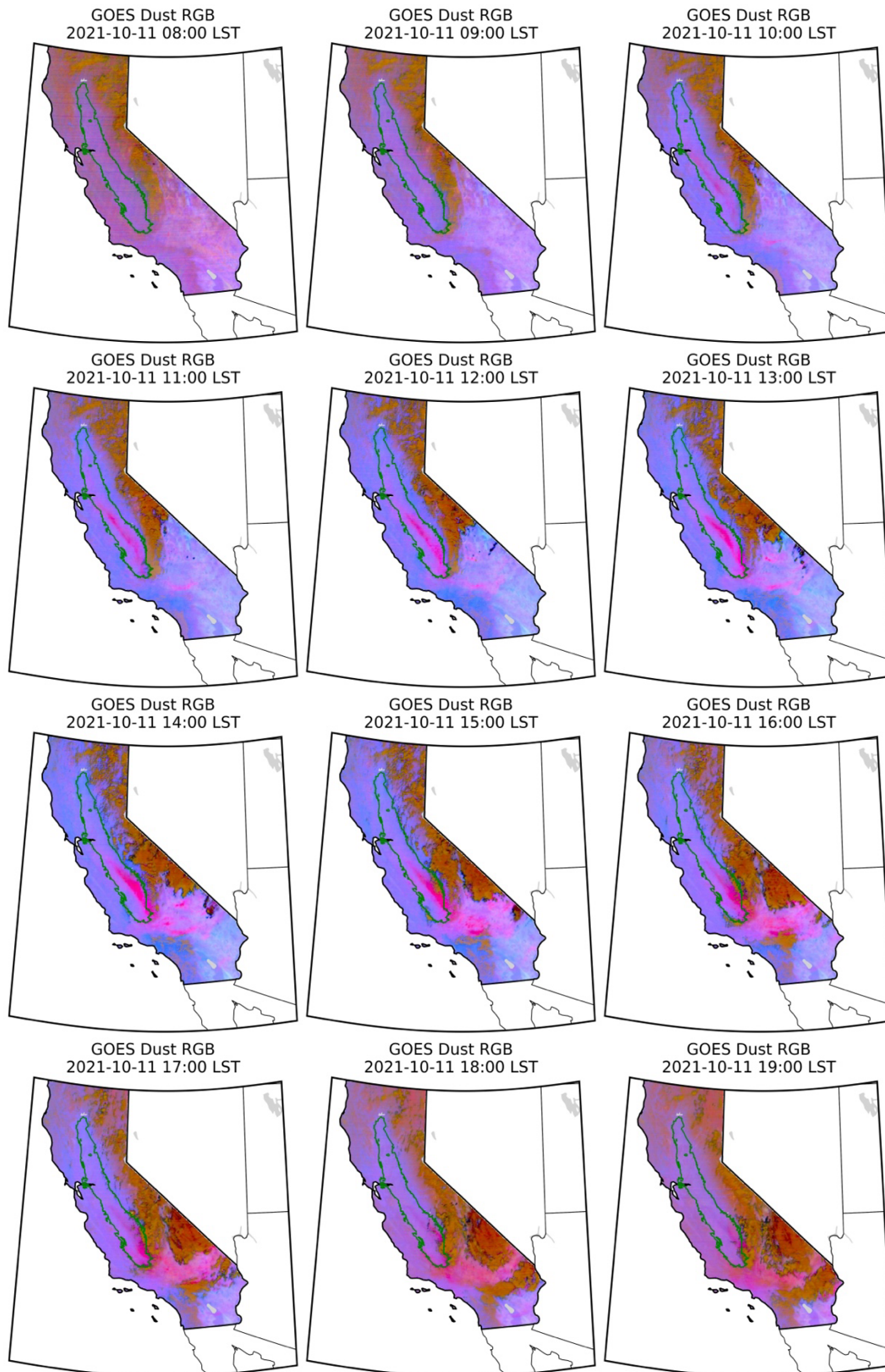
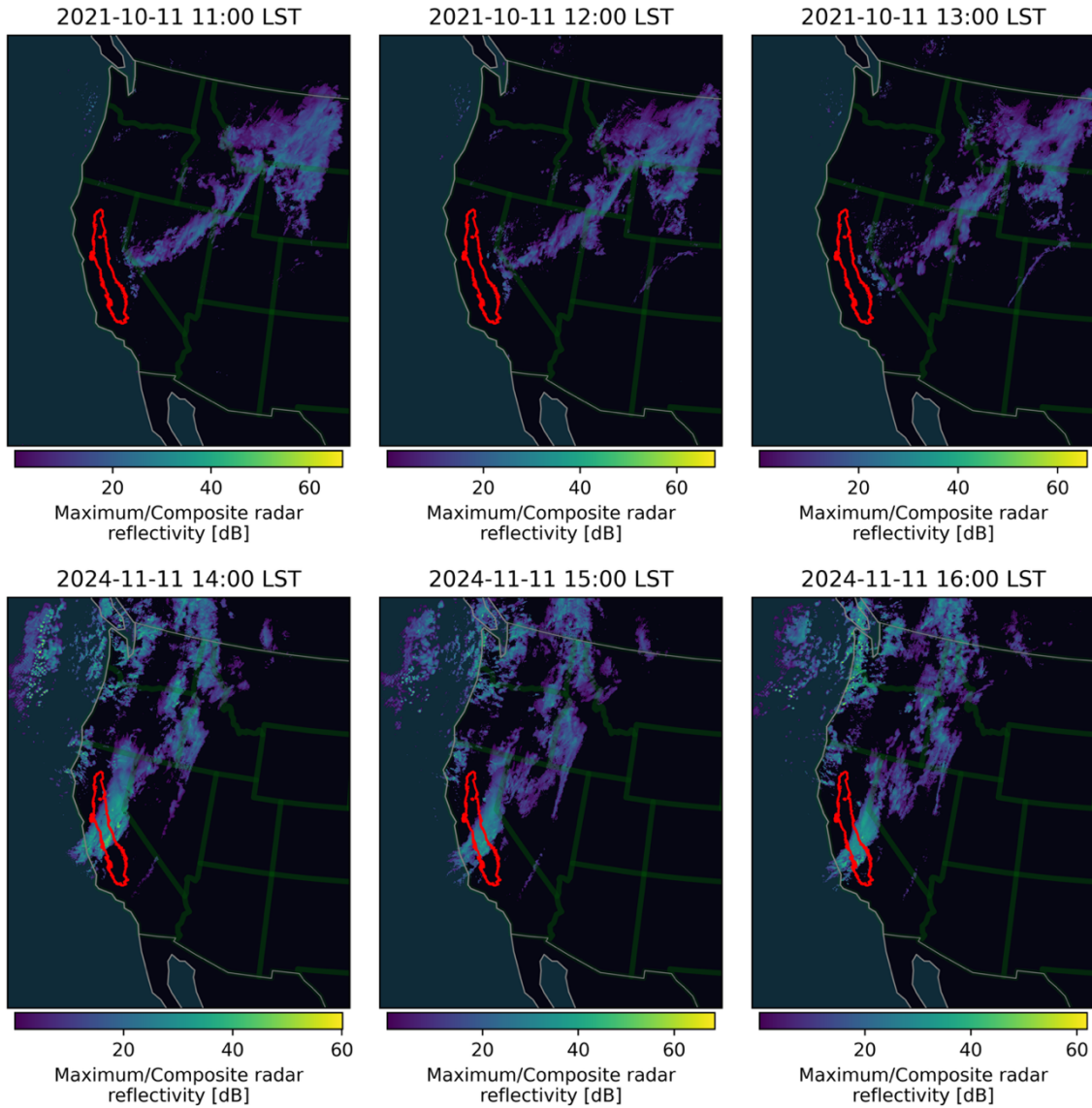
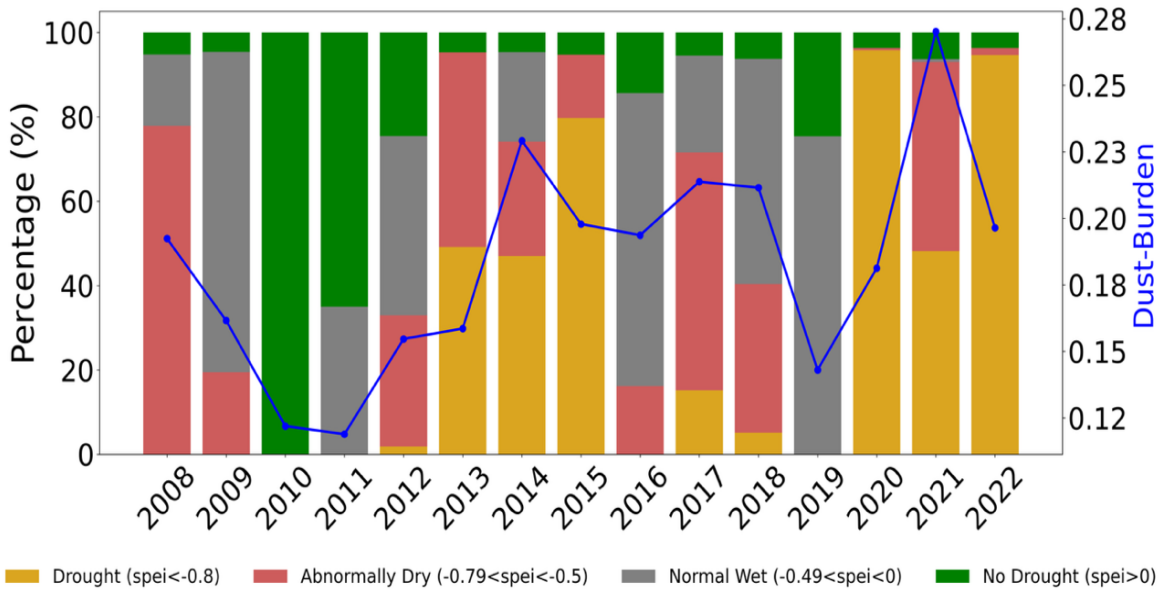


Figure S2. Extended GOES Dust Plume on October 11, 2021.

1138
1139
1140



1141
 1142 **Figure S3.** Hourly composite radar reflectivity during two California Central Valley dust events:
 1143 October 11, 2021 (top) and November 11, 2024 (bottom). The Central Valley dust domain is
 1144 outlined in red. Times are local standard time (LST).
 1145
 1146
 1147
 1148
 1149
 1150
 1151
 1152
 1153
 1154
 1155



1157
 1158
 1159
 1160
 1161
 1162
 1163
 1164
 1164
 1165
 1166
 1167
 1168
 1169
 1170
 1171
 1172
 1173
 1174
 1175
 1176
 1177
 1178
 1179
 1180
 1181
 1182
 1183
 1184

Figure S4. Yearly drought severity class and dust burden in California’s Central Valley, 2008-2022. Stacked bars indicating the percentage fraction of SPEI classes per year. The blue line (right axis) is the annual mean dust burden index. Dust burden tends to increase in drought-dominated years (2014, 2015, 2020, 2021).

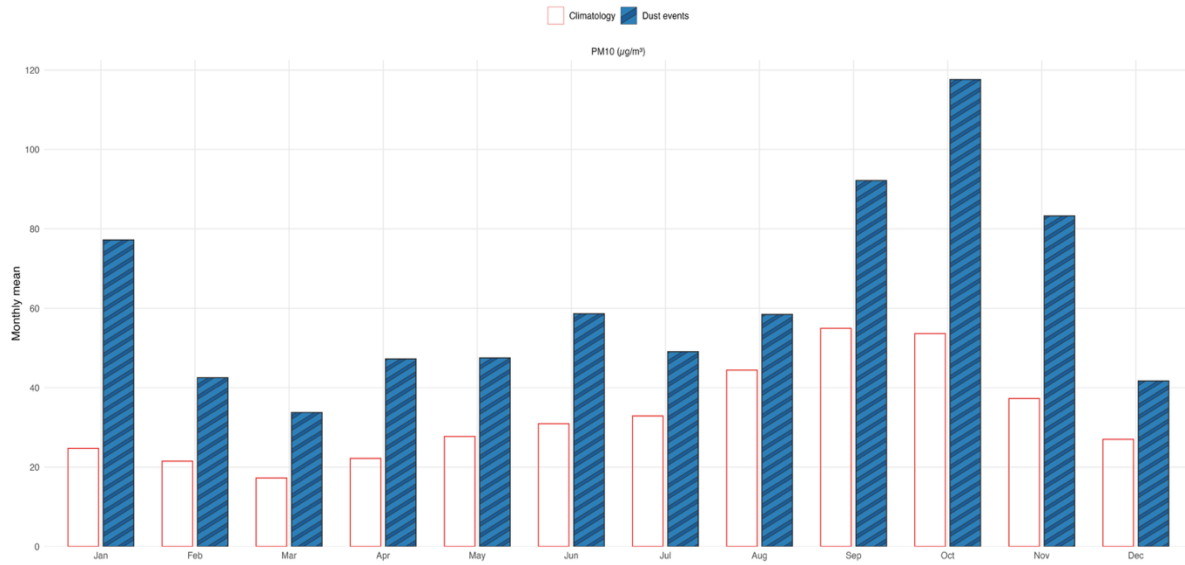


Figure S5. Monthly mean PM10 concentrations ($\mu\text{g m}^{-3}$) on dust events (blue bars) relative to climatology mean (red).

1185
 1186
 1187
 1188
 1189
 1190
 1191
 1192
 1193
 1194
 1195
 1196
 1197
 1198
 1199
 1200
 1201
 1202
 1203
 1204
 1205
 1206
 1207
 1208
 1209
 1210
 1211
 1212
 1213
 1214

1215
1216

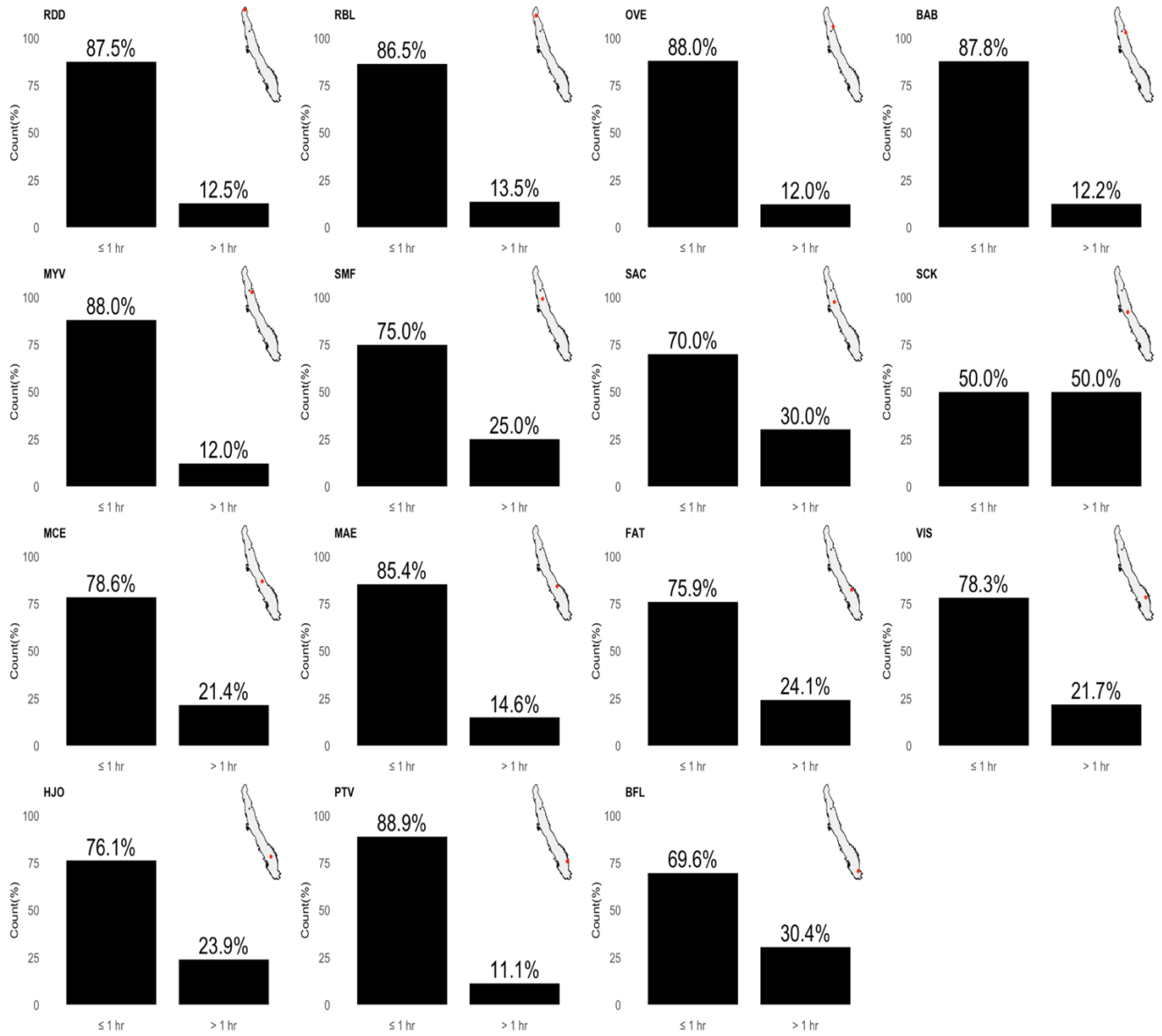
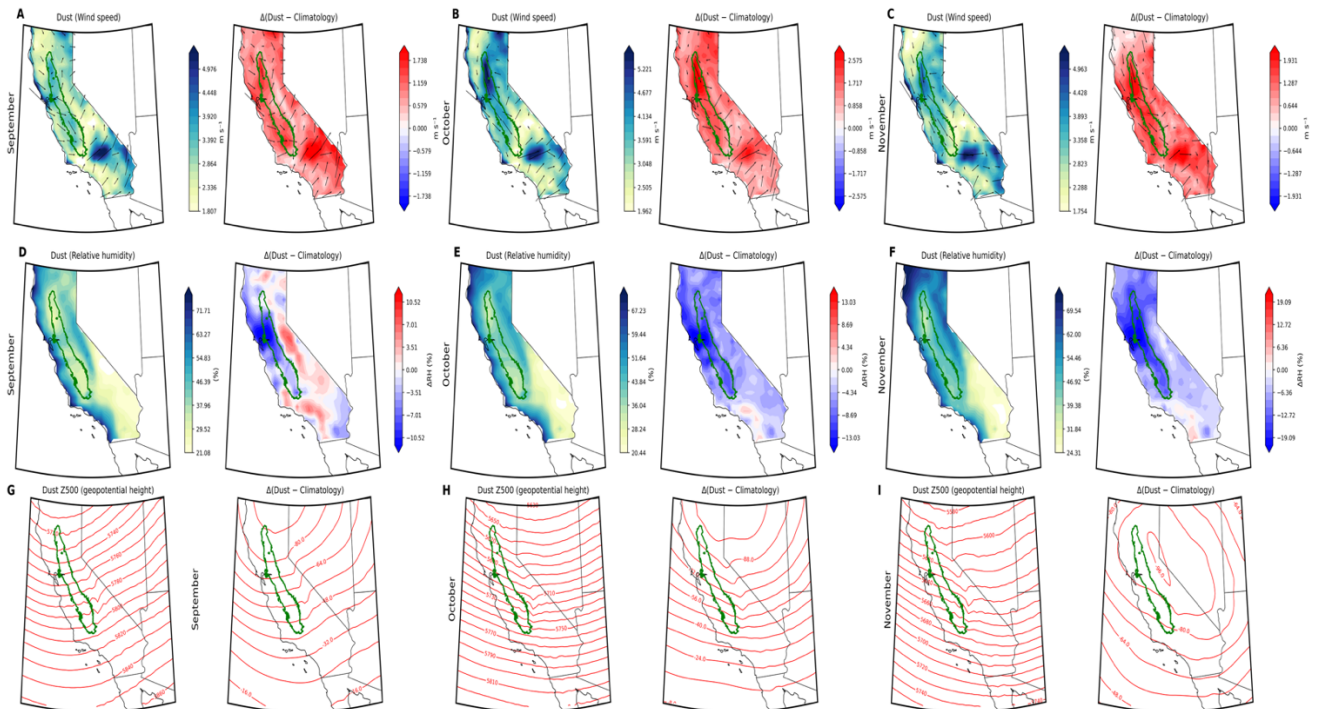


Figure S6. hourly duration of dust event across the Central Valley.

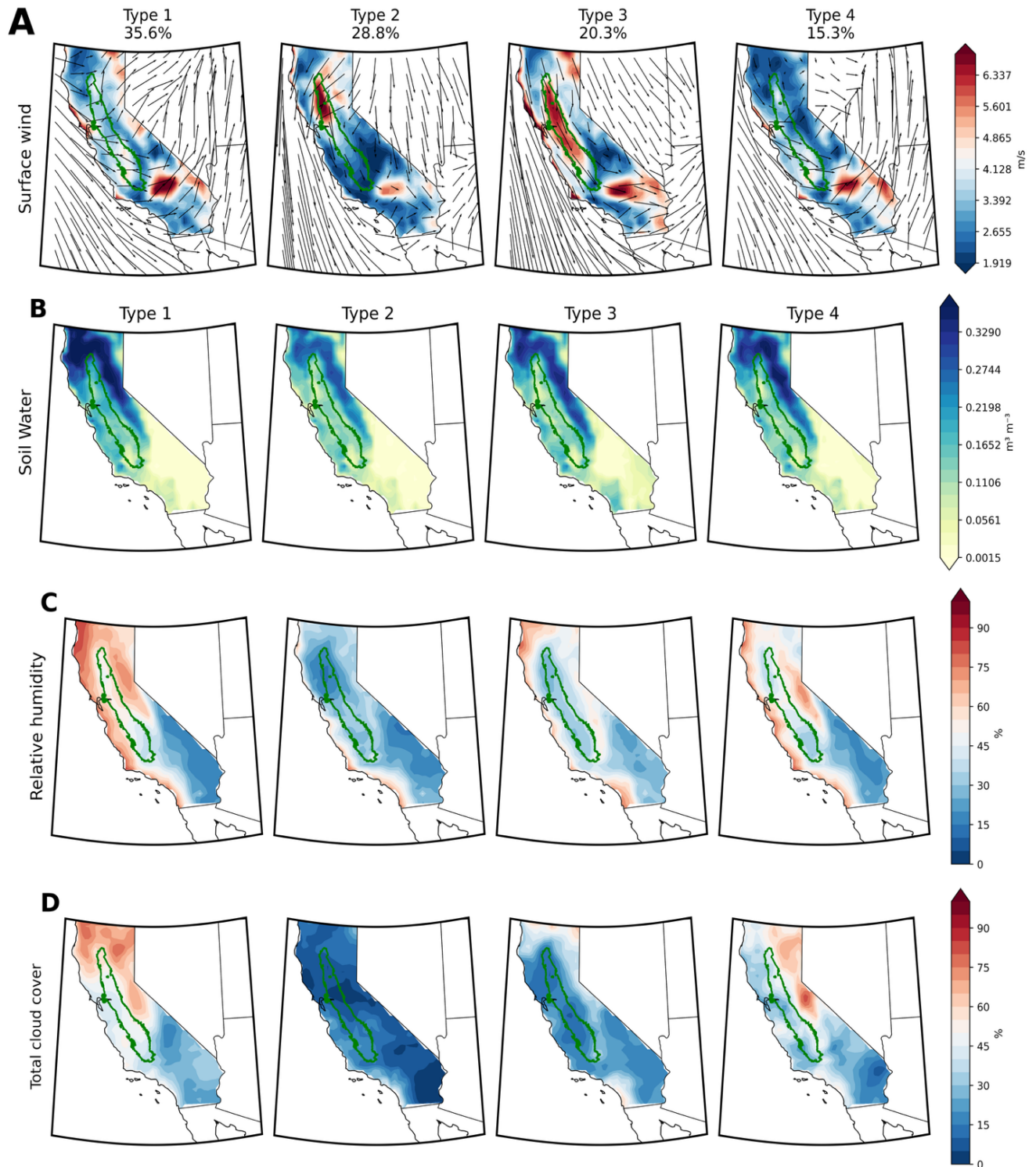
1217
1218
1219
1220
1221
1222
1223
1224
1225
1226
1227
1228
1229

1230
1231
1232



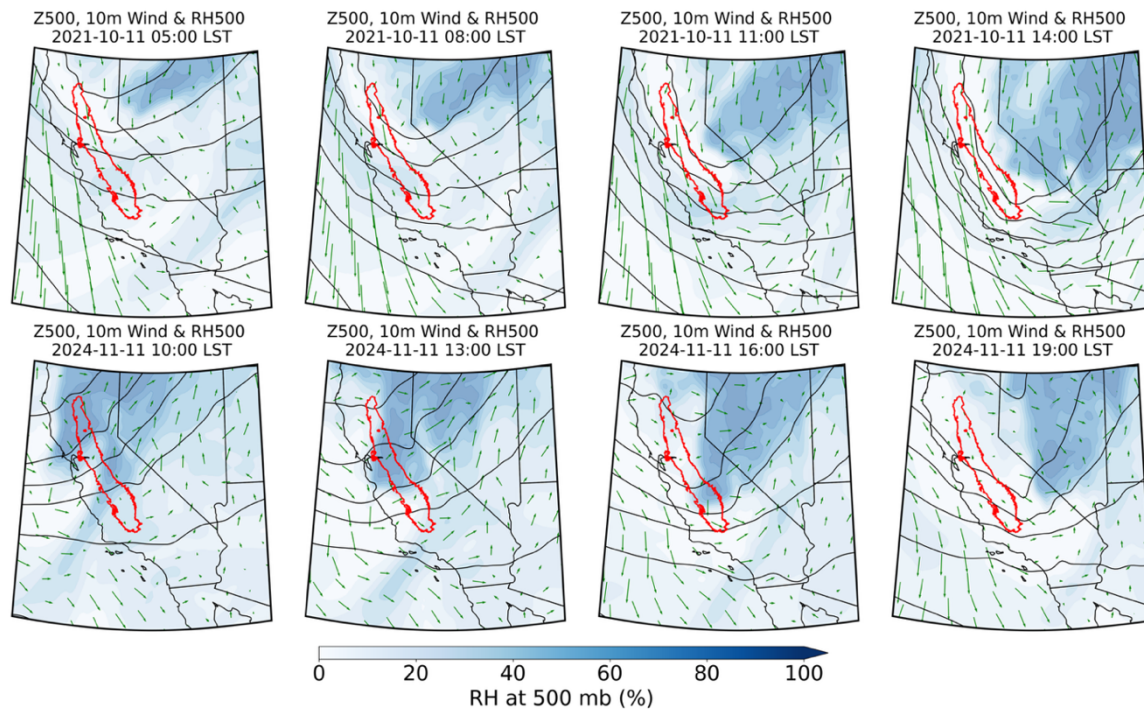
1233
1234
1235
1236
1237
1238
1239
1240
1241
1242
1243
1244
1245
1246
1247
1248
1249
1250
1251
1252
1253
1254
1255

Figure S7. September-November composites of meteorological conditions during Central Valley dust days. For each month (columns), the left subpanel shows the dust day mean, and the right subpanel shows the anomaly relative to climatology. (a-c) surface wind (m/s); (d-f) relative humidity (%); (g-i) 500hpa geopotential (m) (contours). Green outline marks the Central Valley domain.



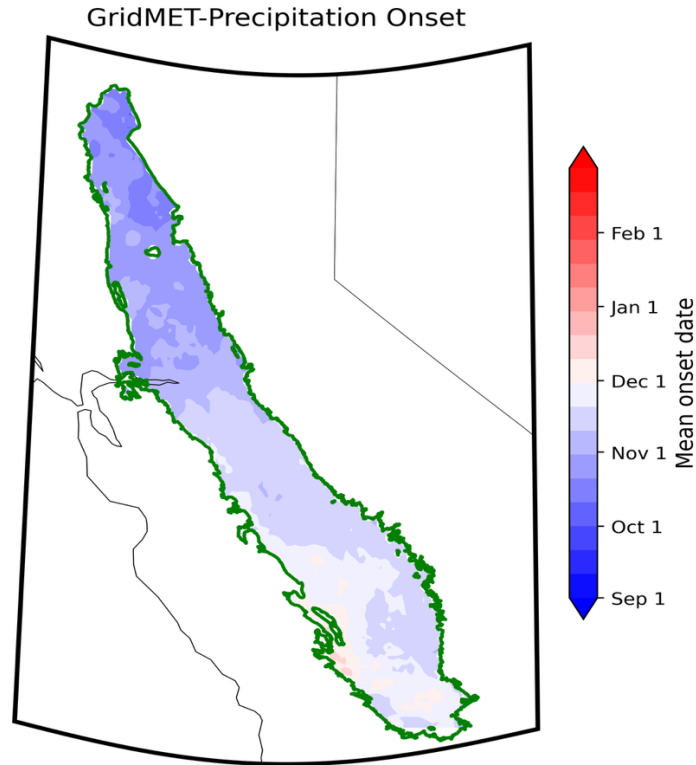
1257
 1258
 1259
 1260
 1261

Figure S8. Dust favorable environment associated with four dominant circulation types as identified in fig 7a. Columns show Type 1-4; rows show dust composites mean of (a) surface wind (m/s), (b) surface soil water ($m^3 m^{-3}$) (c) relative humidity (%), and (d) total cloud cover (%). The green outline marks the Central Valley dust domain.



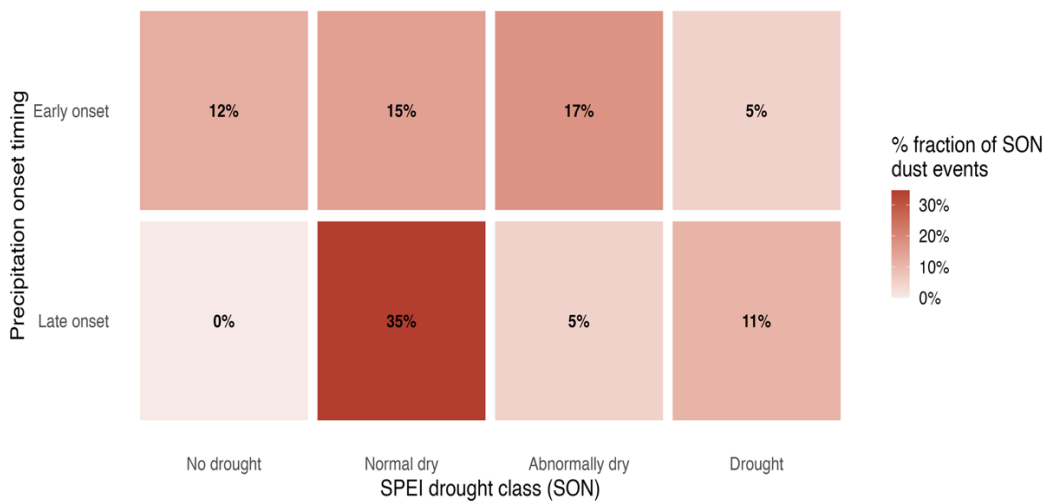
1262
1263
1264
1265
1266
1267
1268
1269
1270
1271
1272
1273

Figure S9. Synoptic evolution of two dust event cases. Panels show 500hpa geopotential (black contours), surface wind vectors (green arrows), and 500hpa relative humidity (blue shading) during October 11, 2021 (top) and November 11, 2024 (bottom). The red outline marks the Central Valley dust domain.



1274
1275
1276
1277
1278
1279

Figure S10. Mean onset date of the first significant rainfall event in the Central Valley (2005-2024).



1280
1281
1282
1283
1284

Figure S11. Seasonal modulation of Central Valley dust events. Panel shows a 2 x 4 grid pairs the Precipitation onset timing (early and late phases) with drought categories. Center values is the % fraction of dust events as a function of SPEI class.

1285 **Table S1.** Locations of meteorological stations used in this study.

Station ID	Airport location	Latitude	Longitude
RDD	Redding Municipal Airport (Redding)	40.509	-122.2934
RBL	Red Bluff Municipal Airport (Red Bluff)	40.1519	-122.2536
OVE	Oroville Municipal Airport (Oroville)	39.49	-121.62
BAB	Beale Air force base (Marysville)	39.13609	-121.4366
MYV	Yuba County Airport (Marysville)	39.10203	-121.5688
SMF	Sacramento International Airport	38.69542	-121.5908
SAC	Sacramento Executive Airport	38.5069	-121.495
SCK	Stockton Metropolitan Airport (Stockton)	37.89417	-121.2383
MCE	Merced Regional Airport (Merced)	37.28603	-120.5179
MAE	Madera Municipal Airport (Madera)	36.98486	-120.1107
FAT	Fresno Yosemite International Airport (Fresno)	36.78	-119.7194
VIS	Visalia Municipal Airport (Visalia)	36.31867	-119.3929
HJO	Hanford Municipal Airport (Hanford)	36.31139	-119.6232
PTV	Porterville Municipal Airport (Porterville)	36.02732	-119.0629
BFL	Meadows Field (Bakersfield)	35.4244	-119.0542

1286 **Table S2.** Locations of PM10 stations used in this study.

EPA ID	Location	Latitude	Longitude
060311004	Hanford-S Irwin Street	36.314399	-119.64457
061010003	Yuba City (Almond Street)	39.138773	-121.618549
060290014	Bakersfield	35.35661	-119.06261
060195001	Fresno (Clovis Villa Avenue)	36.819449	-119.716433
060392010	Madera (28261 Avenue)	36.953256	-120.034203
060472510	Merced	37.30832	-120.48046
060190011	Fresno Garland	36.78538	-119.77321
060670014	Sacramento (Goldenland Ct)	38.650783	-121.506767
060674001	Sacramento (2221 Stockton)	38.556326	-121.458499
060772010	Manteca (530 Fishback Rd)	37.793392	-121.247874
061072002	Visalia	36.332179	-119.291228

1287

1288

1289

1290

1291